Differential modification of the C-terminal tails of different α-tubulins and their importance for microtubule function *in vivo*

Mengjing Bao, Ruth Dörig, Paula Vazquez-Pianzola, Dirk Beuchle, and Beat Suter

Institute of Cell Biology, University of Bern, Switzerland

Summary

1. α-tubulin glutamylation was established in the C-terminal domain of *Drosophila* αTub84B and αTub84D (αTub84B/D). Multiple glutamyl residues were pinpointed in this domain. The female germline α-tubulin, αTub67C, is, however, not glutamylated.
2. *TTLL5* is required for mono- and poly-glutamylation of αTub84B/D.
3. *TTLL5* is required for the proper Kinesin heavy chain (Khc) distribution in the germline, and the kinesin-based refinement of Staufen localization and ooplasmic streaming during late oogenesis.
4. *TTLL5* is needed for the pausing of anterograde trafficking of mitochondria in axons.

Abstract

Microtubules (MTs) are built from α-/β-tubulin dimers and used as tracks by kinesin and dynein motors to transport a variety of cargos, such as mRNAs, proteins, and organelles, within the cell. Tubulins are subjected to several post-translational modifications (PTMs). Glutamylation is one of them, and it is responsible for adding one or more glutamic acid residues as branched peptide chains to the C-terminal tails of both α- and β-tubulin. However, very little is known about the specific modifications found on the different tubulin isotypes *in vivo* and the role of these PTMs in MT transport and other cellular processes *in vivo*. In this study, we found that in *Drosophila* ovaries, glutamylation of α-tubulin isotypes occurred clearly on the C-terminal ends of αTub84B and αTub84D (αTub84B/D). In contrast, the ovarian α-tubulin, αTub67C, is not glutamylated. The C-terminal ends of αTub84B/D are glutamylated at several glutamyl side chains in various combinations. *Drosophila TTLL5* is required for the mono- and poly-glutamylation of ovarian αTub84B/D and with this for the proper localization of glutamylated microtubules. Similarly, proper Kinesin-1 distribution in

the germline also depends on *TTLL5* as well as the refining of Staufen localization and the normal fast ooplasmic streaming with its directional movement, two processes known to depend on Kinesin-1 activities. In the nervous system, the pausing of anterograde axonal transport of mitochondria is affected by an enzymatically dead mutant of *TTLL5*. Our results demonstrate *in vivo* roles of *TTLL5* in differential glutamylation of α-tubulins and point to the *in vivo* importance of α-tubulin glutamylation for Kinesin-1-dependent processes.

Introduction

Microtubules (MTs) are fundamental cytoskeletal filaments comprising heterodimers of α- and β-tubulins. Despite their high level of conservation in eukaryotes, MTs are still quite diverse because cells express different tubulin genes and proteins, which can undergo several different post-translational modifications (PTMs). Based mainly on *in vitro* assays, these variants are thought to optimize the MT interaction with different microtubule-associated proteins (MAPs) and motors.

Drosophila melanogaster possesses four α-tubulin genes. Three of them are expressed during oogenesis and early embryogenesis, suggesting that they contribute to the formation of microtubules during these stages. The three genes are *αTub84B*, *αTub84D,* and *αTub67C* (Kalfayan and Wensink, 1982). αTub84B and αTub84D differ in only two amino acids. Their primary sequence in the C-terminal domain is identical, and both are expressed in most tissues and throughout development. In contrast, αTub67C is expressed exclusively during oogenesis, where it is maternally loaded into the egg and embryo. The primary structure of αTub67C is distinctively different from αTub84B/D (Theurkauf et al., 1986). These differences are also apparent in the C-terminal domain and include the last residue, phenylalanine (Phe, F) in αTub67C and tyrosine (Tyr, Y) in αTub84B/D. *αTub85E* is the fourth α-tubulin. It is mainly expressed in the testes but not in the ovaries (Kalfayan and Wensink, 1982).

MTs are subjected to several PTMs, including the C-terminal tail glutamylation, glycylation, and detyrosination / tyrosination. Furthermore, acetylation and phosphorylation in the more central parts of the tubulins have also been identified (Arce et al., 1975; Eddé et al., 1990; Hallak et al., 1977; L'Hernault and Rosenbaum, 1985; Magiera and Janke, 2014; Redeker et al., 1994). Glutamylation is a PTM that adds one or more glutamic acids (Glu, E) to the side chains of glutamic acid residues in the C-terminal tails of both α- and β- tubulin,

64 causing the formation of a branched peptide chain (Eddé et al., 1990; Redeker et al., 1992).
65 Glycylation is another PTM that adds glycines to the γ-carboxyl group of glutamic acid
66 residues in the C-terminal region (Redeker et al., 1994). At least in vertebrates, tubulin is
67 also subjected to a particular cycle of de-tyrosination-tyrosination (Preston et al., 1979). In
68 this case, the C-terminal Tyr or Phe of α-tubulin is cyclically removed, resulting in a C-
69 terminal Glu residue, and a new Tyr can be re-added to the new C-term. The enzymes that
70 catalyze glutamylation, glycylation, and tyrosination belong to the Tubulin-tyrosine-ligase-like
71 (TTLL) family (Janke et al., 2005). In *Drosophila melanogaster*, this family encompasses 11
72 genes (flybase.org).

73 MTs have an intrinsic polarity with a plus and a minus end. On these tracks, kinesin
74 motors transport cargo to the plus ends, and dynein motors move cargo toward the minus
75 ends. Evidence for the importance of PTMs of tubulin subunits has already been reported *in*
76 *vitro.* Artificial tethering of 10E peptides to the side chains at position E445 of α-tubulin and
77 E435 of β-tubulin by maleimide chemistry increased the processivity (the run length) of
78 kinesin motors on tubulin. For Kinesin-1, this was a 1.5-fold increase (Sirajuddin et al.,
79 2014). In contrast to kinesin, Dynein/dynactin motors preferred a Tyr at the C-term of α-
80 tubulin to initiate processive transport *in vitro* because the motor favored this isotype as an
81 attachment point to dock onto the MTs (McKenney et al., 2016). Recent work now also
82 demonstrated a role for the mouse tubulin glycylation enzymes. *In vitro* fertility assays
83 showed that the lack of both *TTLL3* and *TTLL8* perturbed sperm motility, causing male
84 subfertility in mice. Structural analyses further suggested that loss of glycylation perturbed
85 the coordination of axonemal dynein, thus affecting the flagellar beat (Gadadhar et al.,
86 2021).

87 *CG31108* is considered to be the homolog of the mammalian *TTLL5* gene and was
88 therefore named *DmTTLL5 or TTLL5* (Devambez et al., 2017). It is required for α-tubulin
89 glutamylation in the *Drosophila* nervous system (Devambez et al., 2017). The murine TTLL5
90 is composed of an N-terminal core tubulin tyrosination ligase-like (TTLL) domain, a cofactor
91 interaction domain (CID), and a C-terminal receptor interaction domain (RID) (Lee et al.,
92 2013). The N-terminal core domain was shown to provide the catalytic activity of TTLL5 and
93 is highly conserved in *Drosophila* TTLL5 (van Dijk et al., 2007, Natarajan et al., 2017) (**Table**
94 **1**). According to FlyBase data, *Drosophila TTLL5* mRNA is expressed at high levels in
95 ovaries (**Table S1**), even higher than in the nervous system where initial studies were
96 performed (Devambez et al., 2017). We thus focused on *TTLL5*'s possible functions during
97 *Drosophila* oogenesis to shed light on possible *in vivo* roles of glutamylated α-tubulins.

98 An *in vivo* mouse study showed that the absence of TTLL1-mediated polyglutamylation of
99 α-tubulin increased the overall (both anterograde and retrograde) motility of mitochondrial
100 transport in axons (Bodakuntla et al., 2021). However, another study in *Drosophila* showed
101 that the vesicular axonal transport was not affected by the absence of TTLL5-mediated MT
102 glutamylation in the segmental nerves of larvae (Devambez et al., 2017). Inspired by these
103 controversial results, we also studied the function of *TTLL5* in a second tissue, the adult
104 *Drosophila* wing nerves.

105 Our results revealed that *TTLL5* is essential for the normal glutamylation of the ovarian
106 αTub84B/D. Surprisingly, even in wild-type ovaries, the oogenesis-specific aTub67C was not
107 glutamylated, suggesting that this gene, *αTub67C,* may have evolved to produce MTs that
108 contain regions that are less glutamylated. We found that *TTLL5* is required for the proper
109 distribution of Kinesin heavy chain (Khc), for proper cytoplasmic streaming during late
110 oogenesis as well as for fine-tuning the localization of the Staufen protein. Furthermore,
111 *TTLL5* has a clear effect on the pausing of mitochondria during anterograde axonal transport
112 in wing nerves. Our work, therefore, reveals the *in vivo* importance of glutamylation of
113 specific α-tubulins.

114

115 **Results**

116 **Specific glutamylation on multiple Glu residues of αTub84B/D, but not αTub67C in**
117 **ovaries**

118 Mass spectrometry was performed to analyze the glutamylation of the C-terminal tails of α-
119 tubulins *in vivo*. Proteins extracted from ovaries were purified through SDS-PAGE, and α-
120 tubulin bands were cut out and digested with the protease trypsin-N. C-terminal peptides of
121 the different α-tubulin isotypes were then analyzed for post-translational modifications by
122 liquid chromatography-mass spectrometry (LC-MS). Because the resulting C-terminal
123 peptides are identical between the αTub84B and αTub84D, we refer to them as αTub84B/D
124 (**Fig. 1A**). Analyses of wild-type ovarian extracts revealed that the general *Drosophila* α-
125 tubulins αTub84B/D, but not the ovarian-specific αTub67C, showed glutamylation on their C-
126 terminal tails (**Fig. 1A**). For αTub84B/D, side chain glutamylation was identified on all four
127 glutamyl residues in the tail region, Glu443, Glu445, Glu448, and Glu449. The most
128 extended side chains identified were 3Es in wild-type ovaries **(Fig. 1A,1B)**. According to
129 FlyBase, *αTub84B+D* mRNAs are 4.7x as highly expressed as *αTub67C*. We identified a
130 similar ratio (4.6x) of C-terminal peptides by the MS analysis (**Table S2**). Because of the

131 lower abundance of Tub67C C-terminal peptides, we cannot rule out that rare glutamylation
132 on the maternal αTub67C exists. Altogether, we conclude that glutamylation of α-tubulin had
133 a strong preference for the C-terminal domain of αTub84B/D.

134 ***Drosophila TTLL5* is required for MT mono- and polyglutamylation of ovarian**
135 **αTub84B/D.**

136 To study the function of TTLL5, distinct *TTLL5* loss-of-function mutations were created and
137 characterized (**Fig. 2A**). The *TTLL5*^{pBac} and *TTLL5*^{Mi} mutant strains carry a piggyBac and a
138 Minos transposon, respectively, within the open reading frame of *TTLL5*. The *TTLL5*^{MiEx}
139 mutant was generated by imprecise excision of the Minos element, which caused the
140 formation of a premature stop codon at gene position 8,132 in the open reading frame
141 (codon position 392). An anti-TTLL5 antibody that cross-reacts with additional proteins in
142 ovarian extracts also recognized a band corresponding to the calculated mass of TTLL5.
143 This band was absent in ovarian extracts prepared from the three *TTLL5* mutants,
144 suggesting that they are protein nulls for *TTLL5* or make only a truncated protein (**Fig. 2B**).
145 A transgene containing the wild-type *Drosophila TTLL5* sequence fused to the Venus
146 fluorescent protein sequence under UAS control (UASP-*Venus::TTLL5*) was also produced
147 as a tool to rescue the phenotypes produced by the *TTLL5* mutations and for overexpression
148 studies (**Fig. 2A**).

149 To quantify the effect of *TTLL5* on the glutamylation of the C-terminal tails of α-tubulins,
150 we determined the frequency of C-terminal peptides containing the entire primary sequence
151 and 0, 1, 2, or 3 Glu (E) modifications. This analysis was performed with extracts from wild-
152 type ovaries and the different *TTLL5* mutant ovaries. Wild-type ovaries revealed that 62% of
153 the peptides were modified, 41% with 1E, 14% with 2Es, and 7% with 3Es **(Table 2)**. On the
154 other hand, no glutamylation was observed in *TTLL5*^{pBac} and *TTLL5*^{MiEx} mutants. This clearly
155 shows that *Drosophila TTLL5* is essential for the side chain glutamylation of the C-terminal
156 Glu443, Glu445, Glu448, and Glu449 of αTub84B/D and it appears to affect already the
157 addition of the first Glu.

158 We also measured the levels of monoglutamylation of α-tubulin by Western blotting using
159 the GT335 antibody. This antibody reacts with the first glutamate on the glutamate side-
160 chain even if it is polyglutamylated (**Fig. 3A**) (Wolff et al., 1992). Note that the GT335
161 antibody does not reliably detect all mono glutamylated residues in *Drosophila* tubulins
162 because GT335 preferentially recognizes the first Glu attached to a Glu residue in an acidic
163 environment. In mice, the middle Glu in the sequence -G**E**E- of the C-terminal tail of α-
164 tubulin is such an “acidic” site. Once glutamylated, the branched Glu modification can be

165 recognized by GT335 (Bodakuntla et al., 2021). In contrast, in *Drosophila* α-tubulin, both
166 E443 and E445 in the sequence -G**E**G**E**G- are flanked by Glycines on both sides, which
167 does not provide the acidic environment needed for efficient recognition by GT335. The
168 GT335 signal may, therefore, mainly stem from the glutamylation on the consecutive Glu
169 residues E448 and E449 in the sequence -GA**EE**Y. On Western blots from wild-type
170 extracts, the GT335 antibody produced several bands. The band pointed out by the
171 arrowheads is at the expected position, is reduced or absent in the mutants but reappears in
172 the rescued ovary extracts (**Fig. 3B**). This result, therefore, supports the finding that *TTLL5*
173 is required for monoglutamylation of α-tubulin, and it shows that the antibody signal is
174 specific and can be used to monitor *Drosophila TTLL5* activity.

175 The 1D5 antibody recognizes α-tubulin with an -XEE sequence at the C-terminal α-
176 carboxylate group (with X being a variable residue) (Rüdiger et al., 1999) **(Fig. 3C)**.
177 Therefore, in principle, all Glu residues E443, E445, E448, E449, and the C-terminal Glu
178 residues E448/449 can be recognized if they are not followed by another amino acid (such
179 as Tyr) at their α-carboxylate group. Because *w* control ovaries showed high 1D5 cross-
180 reactivity with a polypeptide of the predicted size, this, therefore, indicates the presence of
181 glutamate side chains containing at least two glutamates and possibly C-terminally de-
182 tyrosinated α-tubulin (Gadadhar et al., 2017; Preston et al., 1979) **(Fig. 3D)**. Consistent with
183 the MS analysis, the *TTLL5* mutants showed a strongly reduced signal with 1D5, indicating
184 that loss of *TTLL5* function prevents normal polyglutamylation. The 1D5 signal was again
185 restored in all *TTLL5* mutants upon expression of the rescue construct. Overexpression of
186 TTLL5 in $TTLL5^{pBac}$ and $TTLL5^{Mi}$ even produced a stronger 1D5 signal and an up-shifted
187 band, suggesting that α-tubulin gets hyperglutamylated **(Fig. 3D)**. These results reveal that
188 *TTLL5* is essential for the glutamylation of the α-tubulin subunit. Moreover, the result that the
189 rescue construct induced the appearance of hyperglutamylated α-tubulin also suggests that,
190 in normal cases, the endogenous *TTLL5* levels are usually limiting in ovaries.

191 Most of the murine TTLL5 residues involved in α-tubulin glutamylation (Natarajan et al.,
192 2017) are conserved in *Drosophila* TTLL5 **(Table 1;** Natarajan et al., 2017**)**. Two are known
193 to be essential for the general enzymatic activity of TTLLs, and two for the interaction with
194 the C-terminal domain of α-tubulin **(Fig. 3E)**. To determine whether these residues are
195 indeed needed *in vivo* for the enzymatic activity of *Drosophila TTLL5* towards αTub84B/D,
196 we used CRISPR/Cas9 to mutate the conserved codons in *Drosophila TTLL5. Drosophila*
197 TTLL5 residues K282 and E517 correspond to mouse K131 and E336*,* respectively*.* They
198 directly interact with ADP/ATP and thus affect general TTLL5 enzymatic activity (Natarajan
199 et al., 2017). $TTLL5^{R339}$ corresponds to mouse $TTLL5^{R188}$*,* which is vital for TTLL5's

200 glutamylation activity. MmTTLL5^{R188} resides in the β6-7 loop, which forms a salt-bridge
201 interaction with the C-terminal tail of α-tubulin and orients it towards the ATP/ADP-binding
202 site (van Dijk et al., 2007). Glutamylation of α-tubulin was impaired in all these *TTLL5*
203 mutants where the conserved residue was replaced **(Fig. 3F)**. Since these mutations did not
204 abolish the stability of the corresponding mutant protein (**Fig. S1**), our results revealed the
205 importance of E517, K282, and R399 of *Drosophila* TTLL5 for glutamylation. Most active site
206 residues of human TTL (Prota et al., 2013; van Dijk et al., 2007) are also conserved between
207 mammalian and *Drosophila* TTLL5 **(Table 3)**. We also mutated the *Drosophila TTLL5*^{P522}
208 codon corresponding to human *TTL*^{P336} (and human *TTLL5*^{P371}/mouse *TTLL5*^{P371}), which is
209 required for anchoring TTL to α-tubulin by forming hydrogen bonds with C-terminal tail
210 residues of α-tubulin (Prota et al., 2013). However, the importance of *TTLL5*^{P371} for
211 glutamylation has not been reported in mammalian systems. Surprisingly, P522 turned out to
212 be essential for the glutamylation of tubulins in *Drosophila* ovaries, revealing P522 as a
213 novel critical residue for the glutamylation function of TTLL5. We also tested whether the
214 overexpression of *TTLL5* in a wild-type background affected polyglutamylation similarly.
215 Indeed, *UASP-Venus::TTLL5* overexpression in ovaries led to hyperglutamylation, as
216 evident from the stronger signal and the additional upshifted band **(Fig. 3G).** All these results
217 point to *TTLL5's* essential role in the glutamylation of α-tubulin.

218 **Other PTMs of the C-terminal tail of ovarian α-tubulin**

219 Western blotting showed no or only minor changes in tyrosinated α-tubulin levels in any of
220 the null or CRISPR/Cas9 generated point mutants, and *TTLL5* overexpression did also not
221 affect these levels **(Fig. 3B, 3F, 3G).** TTLL5 levels, therefore, do not appear to affect levels
222 of tyrosinated α-tubulin in ovaries.

223 Our MS results also detected signals that could correspond to glycylated C-terminal α-
224 tubulin peptides in ovarian samples. Such signals were observed in αTub84B/D but not in
225 αTub67C. However, the standard procedure for the MS analysis involves the alkylation of
226 Cysteine residues in the sample and this procedure can also modify Glu residues, giving rise
227 to the exact same mass change as glycylation (+57.021464 Da; Kim et al., 2016). Our MS
228 analysis could, therefore, not distinguish if a particular Glu residue was artificially modified by
229 carbamidomethylation or naturally by glycylation. To independently test for this PTM, we also
230 performed Western blotting experiments with ovarian extracts and probed them with the anti-
231 mono Gly antibody TAP952 (Bré et al., 1996). Because *TTLL4A* is also expressed in ovaries
232 **(Table S1),** we initially considered it as a potential candidate for performing tubulin
233 glycylation and included mutant samples of *TTLL4A* and *TTLL5* in this analysis. However,
234 even in the wild-type control, the anti-mono Gly antibody TAP952 did not reveal a clear

235 signal at the predicted position (**Fig. S2A**), suggesting that α-tubulin is not glycylated in
236 *Drosophila* ovaries. Furthermore, because the known *Drosophila* polyglycylases (TTLL3A/B)
237 were shown to be the main glycylases in the whole fly and are not expressed in ovaries
238 (Rogowski et al., 2009)(**Table S1**), at present, the combined evidence does not warrant
239 further analysis of this potential PTM in *Drosophila* ovaries.

240 To test for other possible functions of *TTLL4A* in ovaries, ovarian extracts from *TTLL4A*
241 mutants were also blotted and probed with the anti-mono- and polyglutamylation antibodies
242 GT335 and 1D5, respectively. The results showed a strongly reduced signal of both GT335
243 and 1D5 in the ovaries of the $TTLL4A^{pBac}$ mutant, and a weaker reduction of GT335 and 1D5
244 in the $TTLL4A^{pEPgy}$ mutant (**Fig. S2B, S2C**), suggesting the *Drosophila* TTLL4A might
245 function as a glutamylase on α-tubulin in flies. We will discuss the possible interpretations of
246 these results in the Discussion section.

247 **Presence of polyglutamylated microtubules in ovaries**

248 We then analyzed the distribution of polyglutamylated microtubules during oogenesis by
249 immunofluorescence using the 1D5 antibody. Specific 1D5 immunofluorescence signals
250 were observed in the follicle cells and oocytes throughout the previtellogenic, middle, and
251 late oogenesis stages (**Fig. 4**). In the stage 10B (S10B) oocyte, the 1D5 signal showed a
252 slightly biased localization in the cortical region of the oocyte. We observed a robust
253 reduction of the 1D5 signal in *TTLL5* mutant ovaries, revealing that *TTLL5* is essential for the
254 appearance of polyglutamylated microtubules in the ovaries and their concentration at the
255 oocyte cortex in S10B.

256 **Effect of *TTLL5* on the refinement of posterior localization of Staufen**

257 *osk* mRNA localization, combined with translation control, is essential for targeting Osk
258 protein expression to its proper posterior compartment in the cell during mid and late
259 oogenesis (Weil, 2014). Staufen is a protein that associates with *osk* mRNA into a
260 ribonucleoprotein (RNP) complex during *osk* mRNA localization. It therefore also serves as a
261 proxy for *osk* mRNA localization. Staufen/*osk* mRNA localization requires the
262 dynein/dynactin-mediated minus-end transport machinery in the early stages of oogenesis.
263 Subsequently, the Staufen/*osk* mRNA becomes localized to the posterior of the oocyte from
264 the mid to late stages of oogenesis. This particular Staufen/*osk* mRNA localization phase
265 within the oocyte depends on kinesin-driven processes including active transport and
266 ooplasmic streaming in S10B oocytes (Kato and Nakamura, 2012; Lu et al., 2018; Brendza
267 et al., 2000; Zimyanin et al., 2008).

268 To determine whether *TTLL5* contributes to these processes, we studied the role of
269 *TTLL5* in the localization of Staufen in ovaries lacking functional TTLL5. In the wild type, the
270 localization of Staufen appeared very tight on the cortex with little lateral extension in S10B
271 (**Fig. 5A**). In ovaries lacking functional TTLL5, we observed a more diffuse localization
272 pattern of Staufen in the S10B egg chambers of all *TTLL5* null mutants (**Fig. 5B**). Z-stack
273 images revealed a more diffusely spread Staufen signal in the *TTLL5* null mutants, although
274 this varied more between different samples. The increased length of the crescent was fully
275 reversed to the regular length in all UAS-*Venus::TTLL5* rescued strains **(Fig. 5C)**. These
276 results suggest that *TTLL5* is required for tight cortical accumulation of Staufen in S10
277 oocytes. We also analyzed the distribution of Venus::TTLL5 during oogenesis. Antibody
278 staining suggested that Venus::TTLL5 strongly accumulated in the oocyte, especially along
279 the cortex **(Fig. 5C)**. To exclude possible artifacts of the antibody staining, we also tried to
280 observe the self-fluorescent of the Venus tag. Though the Venus fluorescence was relatively
281 weak, Venus::TTLL5 also showed a cortical preference in S10B oocytes, similar to that
282 found by antibody staining (**Fig. S3**). This stronger cortical accumulation of Venus::TTLL5
283 coincides also with the region where polyglutamylated microtubules were enriched at the
284 same stage **(Fig. 4)**.

285 In the *TTLL5* point mutants, where specifically the enzymatic activity of TTLL5 was
286 blocked (*TTLL5*^{E517A}, *TTLL5*^{P522A}, *TTLL5*^{R339A}) the localization pattern of Staufen was not
287 refined and the Staufen signal remained less tightly focused (**Fig. 5D**). An established
288 method to quantify the localization of Staufen to the posterior cortex is to measure the length
289 of the posterior Staufen crescent along the cortex (Lu et al., 2016). A shorter crescent is a
290 sign of tighter localization. Indeed, we found that the length of the posterior Staufen crescent
291 was significantly increased in *TTLL5* null and *TTLL5* point mutant ovaries compared to the
292 control and UAS-*Venus::TTLL5* rescued ovaries (**Fig. 5E)**.

293 We did not observe clear differences in Staufen distribution between the wild type and
294 *TTLL5* mutants in S9 and earlier, previtellogenic stages of oogenesis (**Fig. 5F**). Altogether,
295 these results suggest that the requirement for *TTLL5* for tight cortical accumulation of
296 Staufen starts around S10 and the proper refinement of Staufen localization requires
297 glutamylation of α-tubulin.

298 **The onset of fast ooplasmic streaming requires *TTLL5***

299 Ooplasmic streaming is a process that contributes to the refinement of the posterior
300 localization of Staufen (Lu et al., 2016). It is a bulk movement of the oocyte cytoplasm that
301 circulates and distributes mRNAs and proteins in the oocyte, including the Staufen/*osk*

302 mRNA RNPs. It allows these mRNAs and proteins to reach their intended position, where
303 they become anchored. Ooplasmic streaming can be observed in the mid-stage to the late-
304 stage oocytes. Slow and nondirectional flows initiate at stages 8–9 and are followed by rapid
305 and circular streaming at S10B (Lu et al., 2016). The onset of the fast streaming phase has
306 so far been reported to be attributed to 1) microtubule sliding between stably cortically
307 anchored microtubules and free cytoplasmic microtubules close to the cortex (Lu et al.,
308 2016) and 2) subcortical dynamic microtubule-mediated cargo transport (Monteith et al.,
309 2016). Because the final posterior localization refinement of Staufen in S10B oocytes
310 depends on fast streaming (Lu et al., 2016) and also *TTLL5*, we thus wanted to determine if
311 *TTLL5* contributes to fast ooplasmic streaming.

312 We followed the streaming flow in real-time by measuring vesicle movement in DIC time-
313 lapse movies (**Mov. S1-S5**). We then tracked the movement of the vesicles along the
314 posterior cortical region where microtubule sliding and transport occur (**Fig. 6A**). The
315 kymographs of the tracked vesicles, their analysis, quantification, and interpretation, are
316 shown in **Figs. 6B-6D.** All control ovaries had a typical streaming pattern, and the vesicles
317 were moving unidirectionally parallel to the cortex with a streaming center in the central part
318 of the oocyte. However, 76% *TTLL5*^{MiEx} and all *TTLL5*^{E517A} mutant ovaries displayed
319 abnormal streaming patterns. These abnormal streaming patterns included a partial
320 disruption of streaming especially in the posterior part of the oocyte and a disordered
321 streaming flow in the entire oocyte. The typical streaming pattern was restored in 71%
322 *TTLL5*^{MiEx} ovaries expressing a *Venus::TTLL5* rescue construct. We also evaluated
323 streaming flows in oocytes overexpressing *Venus::TTLL5.* Elevated TTLL5 levels seemed to
324 affect the streaming, too. 29% of the oocytes displayed an abnormal streaming movement or
325 a weak streaming flow like the one observed in *TTLL5* mutants. Moreover, even in oocytes
326 with a circular streaming pattern, the streaming center frequently appeared at a more
327 anterior position in the oocyte, while the cytoplasmic flow in the posterior region was less
328 clearly directed (see **Fig. 6B #2** and **Movie S5 Sample 2**). We thus conclude that the onset
329 of unidirectional fast streaming in S10B oocytes requires moderate levels of *TTLL5*. Again,
330 because abnormal streaming was observed when the enzymatic glutamylation activity of
331 TTLL5 was impaired (*TTLL5*^{E517A}), our results suggest that TTLL5 acts on the ooplasmic
332 streaming through its role in MT glutamylation.

333 ***TTLL5* affects kinesin distribution in the late-stage female germline**

334 Both Staufen/*osk* mRNA localization and ooplasmic streaming depend on kinesin-1-driven
335 processes (Lu et al., 2016) (Serbus et al., 2005) (Brendza et al., 2000). Therefore, we

336 examined whether *TTLL5* somehow affects Kinesin-1. Firstly, the expression levels of
337 ovarian Kinesin heavy chain (Khc) were neither affected by lack of *TTLL5* function (**Fig. 7A**)
338 nor by *TTLL5* overexpression (**Fig. 7B**). Next, we determined the localization of Khc in stage
339 10B, when the fast streaming starts. Even though the MT arrays start to disassemble and re-
340 organize in the S10B oocyte, Khc showed a biased enrichment at the posterior in most wild-
341 type control oocytes (**Fig. 7C**). Out of 37 wild-type oocytes, 76% showed a posteriorly
342 enriched Khc signal (**Fig. 7D**). In contrast, Khc distribution showed a posterior oocyte
343 enrichment in only 13% and 14%, respectively, in $TTLL5^{pBac}$ and $TTLL5^{MiEx}$ mutant egg
344 chambers, respectively (**Fig. 7C and 7D**). Elevated expression levels of *TTLL5* seemed to
345 affect Khc posterior accumulation as well because a smaller fraction of oocytes (54%)
346 displayed clear posterior Khc enrichment than in the control (**Fig. 7C and 7D**). These results
347 demonstrate that moderate levels of *TTLL5* are needed for the proper posterior enrichment
348 of Khc in S10B oocytes.

349 Khc showed an additional higher accumulation in the inner part of the oocytes (arrowhead
350 in **Figs. 7E**) and this was seen in 76% of the oocytes (**Fig. 7F**). We measured the
351 fluorescence intensity of the Khc signal along the anterior-posterior (AP) axis of the oocytes
352 (line in **Fig. 7E).** The signal intensity showed a peak in the center or more posteriorly in wild-
353 type oocytes (**Fig. 7G and S4**), indicating that Khc concentration is higher and Khc might
354 function in these regions of the oocyte. In the *TTLL5* mutants, the inner accumulation of Khc
355 was strongly reduced or absent (**Fig. 7E, 7G, S4**). Only 19% of $TTLL5^{pBac}$ and 14% of
356 $TTLL5^{MiEx}$ oocytes showed a slight inner Khc accumulation (**Fig. 7F**). Overexpressing TTLL5
357 in wild-type oocytes showed an inner peak of Khc accumulation in 65%, which is slightly less
358 than the wild-type control. Besides, the center of the single peak appeared in a more anterior
359 position (**Fig. S4**). Interestingly, the higher levels of *TTLL5* also led to the appearance of two
360 peaks of internal Khc accumulation in the oocyte, an anterior and a posterior one (**Fig. 7E**,
361 **7G, and S4**). These peculiar inner accumulation patterns of Khc upon *TTLL5* overexpression
362 might explain the unusual ooplasmic streaming patterns with a more anterior center and
363 frequent additional, more posterior streaming center, that appeared in oocytes upon *TTLL5*
364 overexpression. Consistent with the requirement of maintaining the normal circular fast
365 streaming, the proper Khc distribution also needed moderate levels of *TTLL5*. This suggests
366 that Khc is causally connected to the fast cytoplasmic streaming, and both Khc localization
367 and Khc-mediated streaming need *TTLL5.*

368 We also evaluated the localization of the Bicaudal-D (BicD) protein during the early stages
369 of oogenesis. BicD is the linker that couples diverse cargos to the dynein/dynactin motor and
370 can thus serve to evaluate the dynein transport (Claussen and Suter, 2005). The expression

371 levels of BicD were not affected by the TTLL5 levels (**Fig. S5A**). Also, BicD localized to the
372 posterior of the oocytes, and the ratio of the oocytes showing posteriorly localized BicD was
373 similar in controls and *TTLL5* mutants (**Fig. S5B and S5C**). In conclusion and as suggested
374 by the normal appearance of the egg chambers (see next paragraph), at least the
375 dynein/dynactin/BicD transport on early oogenesis microtubules does not appear to depend
376 on *TTLL5*.

377 **Female fertility and ovarian development do not require *TTLL5***

378 The dramatic loss of polyglutamylated ovarian α-tubulin and the phenotypes during late
379 oogenesis in *TTLL5* mutants incited us to analyze whether the morphology of the egg
380 chambers from different stages and female fertility were affected in *TTLL5* mutants.
381 However, the lack of *TTLL5* neither caused a significant decrease in hatching rates, nor
382 distinguishable morphological changes in ovaries. The overall MT polarity of stage 10B
383 oocytes was normal in *TTLL5* mutants based on the localization of the polarity markers
384 Gurken and Staufen protein (**Fig. S6**) (Neuman-Silberberg and Schüpbach, 1996; Zimyanin
385 et al., 2007).

386 **The glutamylation activity of *TTLL5* modulates the pausing of anterograde axonal**
387 **transport of mitochondria**

388 Previous studies in *Drosophila* reported that the absence of α-tubulin glutamylation did not
389 seem to be detrimental to the nervous system functions tested in *Drosophila* (Devambez et
390 al., 2017). The wing nerve is an additional, attractive system to monitor organelle transport,
391 such as the movement of mitochondria (Vagnoni and Bullock, 2016) (Hollenbeck and
392 Saxton, 2005). We thus used wing nerves to study the role of *TTLL5* and glutamylation for
393 neuronal transport in the peripheral nervous system by tracking the movement of GFP-
394 labelled mitochondria (Mito::GFP) in the arch of the L1 region which contains bundles of
395 axons (Vagnoni and Bullock, 2016) (**Fig. 8A**). The mitochondria transported towards the
396 thorax (to the right) move by plus-end transport, which is driven by kinesin, whereas
397 mitochondria transported oppositely are transported by dynein (Vagnoni and Bullock, 2016).
398 Time-lapse videos of Mito::GFP movements are shown in **Mov. S6**. Mitochondria are usually
399 transported unidirectionally over a 3 min tracing time. Bidirectionally moving particles were
400 seen, but only rarely. In these cases, they usually moved a short distance toward one
401 direction, suddenly turned back, and ran in the opposite direction. A schematic running
402 pattern is shown in **Fig. 8B.** The start of a run was chosen at the time point when a motile
403 particle began to move away from a stationary position or when it entered the focal plane,
404 and the stop of a run was set when the particle terminated moving or moved out of the focal
405 plane in the given time window. The “pausing” was called when the particle moved with less

406 than 0.2 μm/s within the time window of a “run”. Particles with speeds higher than 0.2 μm/s
407 were considered “trafficking”. Motile mitochondria were manually tracked in both anterograde
408 and retrograde directions. For the anterograde transport, the run length of mitochondria was
409 similar for each “run” between wild-type controls and *TTLL5*^{E517A} (**Fig. 8C**). However, a
410 significant increase was observed in the net velocity in *TTLL5*^{E517A} compared to wild-type
411 controls (**Fig. 8D**). We investigated the reason and found that the absence of enzymatically
412 active *TTLL5* did not alter the trafficking velocity of mitochondria (**Fig. 8E**), but dramatically
413 decreased the total pausing time (1.4 times less) of the anterograde transport of
414 mitochondria (**Fig. 8F**). This suggested that *TTLL5* might not directly affect the trafficking but
415 rather the pausing of mitochondrial transport. To further study the pausing behavior of
416 mitochondria, kymographs of individual motile mitochondria were generated. Kymographs of
417 three representative anterograde transported mitochondria are shown for both genotypes
418 (**Fig. 8G**). The pausing of the mitochondria is pointed out by yellow arrowheads. More
419 frequent pausing was observed in controls compared to the *TTLL5*^{E517A}. By analyzing the
420 pausing number in the given distance, we identified a 1.5 times more frequent pausing in
421 controls compared to the *TTLL5*^{E517A} mutant (**Fig. 8H**). These results indicate that the longer
422 total pausing time in controls was most likely due to more frequent pausing during
423 anterograde transport. The effect of the lack of TTLL5 enzymatic activity on retrograde
424 transport was less clear because we did not observe significant differences measuring the
425 parameters of the retrograde transport. To sum up, these results suggest that the
426 glutamylation activity of TTLL5 is needed for controlling the pausing of this anterograde
427 axonal transport.

428

429 **Discussion**

430 **Glutamylation of the C-terminal tail of ovarian α-tubulin**

431 Side chain glutamylation of the C-terminal domain of α-tubulin in *Drosophila* ovaries was
432 observed using specific antibodies and MS identification. Results from wild-type ovaries and
433 mutants revealed that *TTLL5* is essential for this modification. Consistent with results from
434 mammalian cells and the *Drosophil*a nervous system (Devambez et al., 2017; van Dijk et al.,
435 2007), the strongly reduced or absent Western blot signal of monoglutamylated tubulin in the
436 presumptive null mutants of *TTLL5* **(Fig. 3B)** shows a requirement for *TTLL5* for the
437 accumulation of α-tubulin with the first branching Glu side chain added to one of the C-
438 terminal Glus. The MS analysis led to the same conclusion because it did not uncover any
439 glutamylation in the *TTLL5* mutants. In theory, this could mean that *TTLL5* is required for the

440 addition of this first Glu side chain residue or it might only be required for the stability of
441 glutamylated α-tubulin. TTLL5 has the enzymatic activity to add glutamyl groups and
442 mammalian TTLL5 is considered to be an initiator glutamylase. We can, therefore, assume
443 that the former is the case in *Drosophila*, too. TTLL1 and TTLL6 are elongators of
444 polyglutamylation of α-tubulin (Gadadhar et al., 2017; van Dijk et al, 2007; Janke et al.,
445 2005). However, there is no evidence that the homologous *TTLL6A*/*TTLL6*B or *TTLL1A/1B*
446 are expressed in *Drosophila* ovaries **(Table S1)**. The robust reduction of polyglutamylated
447 tubulin in *TTLL5* mutants observed in ovaries (this work) and the nervous system
448 (Devambez et al., 2017) further shows that *TTLL5* is also needed, directly or indirectly, for
449 polyglutamylation in *Drosophila.* However, we cannot easily figure out *in vivo* if TTLL5 itself
450 has the activity to extend the oligo-Glu side chains. TTLL4A is another enzyme that is
451 expressed in ovaries. Though the predicted mouse homolog of the *Drosophila* TTLL4A
452 prefers to glutamylate β-tubulin (van Dijk et al., 2007; Mahalingan et al., 2020), our data
453 revealed a strong requirement for *Drosophila TTLL4A* for the proper glutamylation of α-
454 tubulin **(Fig. S2C)**, and the Western blotting experiments suggested that it might be required
455 for both monoglutamylation and polyglutamylation **(Figs. S2B and S2C)**. However, the
456 interpretation of the Western blotting results with the GT335 antibody is often difficult and
457 further mass spectrometry analyses should be performed to verify the status of glutamylation
458 of MTs in the mutants.

459 The MS results revealed that glutamylation strongly preferred the substrate αTub84B/D
460 over αTub67C, even though αTub67C is an ovarian-specific α-tubulin. This points to a
461 possible need for a side-chain modification-resistant α-tubulin in the germline to regulate
462 different transport processes by providing local MT sites with reduced side-chain
463 glutamylation, possibly to allow for longer processive movement of kinesin motors as was
464 observed in the absence of glutamylation in the mitochondrial transport assay **(Fig. 8)**. It will
465 also be interesting to find out whether MT tracks containing specific hypoglutamylated
466 regions exist in oocytes and whether these perform an important function in large insect
467 oocytes that use rapid cytoplasmic streaming to localize patterning factors.

468 **Function of glutamylation of microtubules on Kinesin-1 dependent streaming in late-**
469 **stage oocytes**

470 The unidirectional flow seen during rapid ooplasmic streaming is caused by the Kinesin-1-
471 dependent MT sliding and MT cargo transport along the cortical and subcortical MTs (Lu et
472 al., 2016) (Monteith et al., 2016). The proper localization of Khc to the posterior cortical
473 region **(Fig. 7)** and the glutamylation of cortical MTs **(Fig. 4**) depend on TTLL5*,* which is

474 normally also concentrated at the cortex in S10B oocytes (**Fig. 5C** and **Fig. S3**). The
475 observation of these correlations in the cortical region point to the glutamylation of the MTs
476 as a precondition for the proper localization and function of Kinesin-1.

477 Kinesin-1 also accumulates at higher levels in the inner part of the oocyte (**Fig. 7**),
478 suggesting that the inner-oocyte MTs might also contribute to the rapid streaming observed.
479 This hypothesis is supported by the observation that hyperglutamylation by TTLL5
480 overexpression often leads to an anterior-biased accumulation of Khc in the interior of the
481 oocyte or the formation of two inner Khc clusters along the anterior-posterior axis (**Figs. 7E,**
482 **G**, **Fig. S4**). This abnormal Khc distribution is then mirrored by the streaming pattern in such
483 oocytes (**Fig. 6D**), suggesting that it may cause the shift of the streaming center to the
484 anterior part of the oocytes and the appearance of a second posterior streaming center.
485 Further investigations through direct tracking of Khc movement in S10B oocytes under hypo-
486 and hyperglutamylation conditions may provide more insight into the impact of MT
487 glutamylation on Kinesin-1 function *in vivo.*

488 **Role of glutamylation of α-tubulin for stopping transported mitochondria**

489 The previous study showed that α-tubulin was the only tubulin subunit that can be
490 glutamylated in the *Drosophila* nervous system and *TTLL5* is required for α-tubulin
491 glutamylation in the neurons (Devambez et al., 2017). However, the absence of *TTLL5* did
492 not reveal clear defects in larval neuromuscular junction morphology, larval locomotion
493 behavior, or vesicular axonal transport in larval neurons. We, therefore, used a different
494 system, the transport of mitochondria in the adult wing axon to test for a possible neuronal
495 function.

496 By measuring the parameters related to the pausing time and pause frequency, we found
497 that the normal stopping or pausing of mitochondria during axonal transport needs *TTLL5*
498 and its glutamylase activity, suggesting that glutamylated α-tubulins are needed for this
499 effect. Glutamylated side chains of α-tubulin might act as marks or even obstacles that
500 disturb the movement of mitochondria. Consistent with our results, a previous *Drosophila*
501 *TTLL5* study mentioned that a slight effect on pausing of vesicles during axonal transport
502 had also been noted in *TTLL5* mutants but turned out to be not significant (Devambez et al.,
503 2017). Additionally, a recent study revealed a similar function of glutamylation of α-tubulin for
504 the transport of mitochondria (Bodakuntla et al., 2021). The absence of polyglutamylation of
505 α-tubulin in *TTLL1*$^{-/-}$ increased the motility of mitochondria in the mouse neurons but did not
506 affect their transport velocity. The results led to the hypothesis that glutamylation of α-tubulin

507 may not directly affect transport but rather affect mitochondrial docking and motor binding to
508 MT tracks by acting as roadblocks on the MT tracks.
509 Our results showed a selective effect of Glu-MTs on mitochondrial motility for plus-end
510 transport in axons, a process that is carried out by Kinesin-1 (Pilling et al., 2006). This
511 suggests that glutamylation of MTs plays a role in controlling Kinesin-1 activity similar to
512 what we had observed in the stage 10B oocyte. Several *in vitro* studies have also shown that
513 Glu-MTs affect Kinesin-1 activity. The considerable negative charge of the modified regions
514 in the poly-Glu-modified tubulins might interfere with the interaction of kinesin with tubulin
515 (**Fig. 1B;** Skiniotis et al., 2004). *In vitro* studies demonstrated that the artificial tethering of
516 glutamyl peptides to the side chains of MTs affected the function of Kinesin-1 (Sirajuddin et
517 al., 2014). More recent *in vitro* studies further reveal that TTLL7-modified β-tubulin
518 polyglutamylation specifically decreases the motility of Kinesin-1 (Genova et al., 2023). All
519 these observations suggest that side chain glutamylation of MTs is sensed by Kinesin-1 and
520 functions to interfere with the MT binding of Kinesin-1, thus disturbing the movement of
521 Kinesin-1 dependent cargos. However, an alternative hypothesis is suggested by the work of
522 Lacroix and colleagues (Lacroix et al, 2010). They showed that glutamylation of MTs leads
523 to the breakage of the "MT road" by recruiting severing proteins and this is then followed by
524 the disruption of cargo transport. These studies showed that the severing rate of a
525 microtubule severing protein Spastin was increased in the presence of MTs that were
526 glutamylated by TTLL4 or TTLL6 in cultured HeLa cells. Another group demonstrated that
527 the glutamylated MTs (modified by TTLL7) increased Spastin-mediated severing when
528 glutamic acid side chains were shorter than 8Es (Valenstein and Roll-Mecak, 2016), which is
529 the case in *Drosophila* ovaries **(Fig. 1)**. A second MT severing protein has recently entered
530 the scene in the same context. The interaction of Katanin with microtubules is also enhanced
531 by α-tubulin tail glutamylation in *C. elegans* (Szczesna et al., 2022). *Drosophila* Spastin is
532 present in the axons and synaptic connections of larvae. However, the effects of its absence
533 in *Drosophila* larval neurons are controversial. One group suggests that the loss of Spastin
534 leads to a reduction in synapse growth and an increase in synaptic transmission (Trotta et
535 al., 2004), while another study reports the opposite effect (Sherwood et al.,
536 2004). *Drosophila* Katanin acts as a severing protein and is required for proper synapse
537 development in the larval neuromuscular junction (NMJ; Díaz-Valencia et al., 2011; Mao et
538 al., 2014). It would also be valuable to investigate the impact of broken MTs on axonal cargo
539 transport using the adult wing axon system, which presents a unique method to study this
540 phenomenon. Because α-tubulin is the major substrate for glutamylation in
541 the *Drosophila* nervous system, this system is a powerful and simple *in vivo* model to study
542 in greater detail the effect of glutamylation of these specific α-tubulin isotypes on the
543 movement of MT motors.

544 **Physiological relevance of α-tubulin glutamylation**

545 Even though an essential function of α-tubulin glutamylation has not emerged from this
546 study, it has become clear that Kinesin-1-dependent processes are modified or controlled by
547 this modification and that evolution has adapted the tubulin code to optimize the usage of
548 MTs for different evolving needs. That *TTLL5* is not essential for survival also makes this
549 protein an interesting candidate for drugs that can modulate its glutamylation activity to
550 regulate and possibly even increase MT transport in neurodegenerative diseases where MT
551 transport is known to be affected (Bodakuntla et al., 2020)
552

553 **Materials and methods**

554 ***Drosophila* genetics**

555 The fly stocks used in this study, *MattubGal4* (7062), *TTLL5*^{pBac} (16140; allele name
556 *TTLL5*^{B093}), *TTLL5*^{Mi} (32800; allele name *TTLL5*^{MI01917}), and *Df(3R)BSC679* (26531) were
557 obtained from the Bloomington Drosophila stock center. The *TTLL5*^{MiEx} mutation was made
558 by imprecise excision of the Minos element, which left a 3-base insertion (CTA), which
559 introduced a premature stop codon at the genomic position 8,132 in the open reading frame
560 (polypeptide position 392). The different *TTLL5* point mutations were generated by
561 CRISPR/Cas9. The two *Drosophila* stocks used for *TTLL5* gene editing, *y[1] M{w[+mC]=nos-*
562 *Cas9.P}ZH-2A w[*]* and *y[1] v[1] P{y[+t7.7]=nos-phiC31\int.NLS}; P{y[+t7.7]=CaryP} attP40*
563 were obtained from the Bloomington *Drosophila* Stock Center (54591) (Port et al., 2014) and
564 (25709), respectively. Target sequences near the K131, R339 R376, and E517 codons were
565 selected to introduce INDELs and the following point mutations: K131A, R339A (b6-7 loop),
566 R376A, and E517A. Phosphorylated and annealed primers (**Table S3A**) needed to construct
567 the corresponding coding sequences for a single guide RNA (sgRNA) were each cloned into
568 the BbsI site of *pCFD5* according to the protocol published on www.crisprflydesign.org. After
569 amplifying the vector in XL1 blue cells, the plasmids were sequenced to verify the correct
570 assembly. Subsequently, they were injected into *attP40* embryos. *TTLL5*-guide stocks with
571 integrated genes encoding sgRNAs were established *(=v; attP40{v*$^{+}$*, TTLL5-guide}/CyO*). To
572 obtain INDELs for TTLL5, a three-generation crossing schema was set up. Firstly, *nos-cas9*
573 virgins were crossed with males from the different TTLL5-guide stocks. Secondly, the
574 subsequent single male progeny was crossed with *w; Ly/TM3, Sb* virgins. Thirdly, resulting
575 in single *TM3, Sb* males were again crossed with *w; Ly/TM3, Sb* virgins to establish the
576 stocks. The nature of the mutated *TTLL5* alleles was determined by sequencing the targeted
577 region in each stock and comparing it to the sequence of the *TTLL5* gene of the parental *y w*
578 *{w*$^{+}$*, nos-cas9}* mothers and *TTLL5-guide* fathers (**Table S3B).** All the *TTLL5* alleles were
579 crossed to *Df(3R)BSC679* to analyze the effect of the *TTLL5* mutations in hemizygous
580 animals. Abnormally shaped egg chambers were seen in *TTLL5*^{pBac}*/Df(3R)BSC679.* But it
581 seems to be the second site effect as the phenotype disappeared when it was in
582 combination with specific 2nd chromosomes, for example, *MattubGal4/+ or +/UAS-*
583 *Venus::TTLL5).*

584 The *UASp-venus::TTLL5* DNA construct was made from the *TTLL5* cDNA amplified by
585 PCR (forward primer: 5′ - GTTCAGATCTATGCCTTCTTCATTGTGTG -3′; reverse primer: 5′
586 -GAGTCATTCTAGAGCTTCATAGAAATACCTTCTCC- 3′). The resulting DNA was inserted
587 into the *pUASP-venus* vector via Xba I/Bgl II ligation and targeted into the *attP-58A* landing

588 platform (24484) to generate the transgenetic *UASp-venus::TTLL5* fly strain. *ApplGal4* and
589 *UAS-mito::GFP* were kindly provided by Simon Bullock's group (Vagnoni et al., 2016).

590 The *TTLL4A* loss-of-function mutants were *TTLL4A*^{pBac} (17925; allele name *TTLL4A*^{e01119}),
591 *TTLL4A*^{pEPgy} (22659; allele name *TTLL4A*^{EY23195}), and *Df(2L)BSC145* (9505). They were
592 obtained from the Bloomington *Drosophila* stock center. The *TTLL4A*^{pBac} strain carries
593 a piggyBac transposon that had inserted into the leader sequence of *TTLL4A*. The
594 *TTLL4A*^{pEPgy} carries a pEPgy transposon that had inserted into the promotor region of
595 *TTLL4A.* The *Df(2L)BSC145* removes the region that covers *TTLL4A*.

596 **Western blotting**

597 Western blotting performed with ovarian extracts was carried out with 10-20 pairs of ovaries
598 for each genotype. Newly hatched females of the indicated genotypes were collected and
599 crossed with *w* males in fresh vials with ample yeast food for two to three days. Fully
600 developed ovaries were then dissected and collected. The samples were directly lysed in
601 Laemmli buffer, boiled at 95°C for 10 min, fractionated by SDS-PAGE, and transferred onto
602 PVDF membranes. The following primary antibodies were used: mouse 1D5 (1:500,
603 Synaptic System), mouse GT335 (1:200, Adipogen), mouse DM1A (1:1,000, Sigma), mouse
604 tyrosinated α-tubulin (1:1,000, Sigma), rabbit GFP (1:2,000, Sigma), rabbit GAPDH (1:1,000,
605 GeneTex), rabbit *Drosophila* Clathrin light chain (Clc) (1:2,000, Heerssen et al.,
606 2008), mouse BicD (1B11 plus 4C2, 1:5) (Suter and Steward, 1991), rabbit Khc (1:1,000,
607 cytoskeleton), mouse TAP952 (1:500, Merck). For testing the expression of TTLL5, the
608 ovaries were homogenized in ice-cold lysis buffer (150 mM NaCl, 50 mM Tris-HCl (pH 7.5),1
609 mM $MgCl_2$,1 mM EDTA, 0.1% Triton X-100, 0.5 mM DTT, and protease inhibitor cocktail
610 (Roche)) and centrifuged at 13,200g for 20 min. The supernatant with the soluble proteins
611 was collected and loaded for WB. The rabbit anti-Drosophila TTLL5 (1:500) was generated
612 by the GenScript company. The fragment used for antigen induction was:
613 TKLLRKLFNVHGLTEVQGENNNFNLLWTGVHMKLDIVRNLAPYQRVNHFPRSYEMTRKDR
614 LYKNIERMQHLRGMKHFDIVPQTFVLPIESRDLVVAHNKHRGPWIVKPAASSRGRGIFIVNS
615 PDQIPQDEQAVVSKYIVDPLCIDGHKCDLRVYVLVTSFDPLIIYLYEEGIVRLATVKYDRHADN
616 LWNPCMHLCNYSINKYHSDYIRSSDAQDEDVGHKWTLSALLRHLKLQSCDTRQLMLNIEDLI
617 IKAVLACAQSIISACRMFVPNGNNCFELYGFDILIDNALKPWLLEINLSPSMGVDSPLDTKVKS
618 CLMADLLTCVGIPAYS. Secondary antibodies were HRP-linked goat anti-mouse (1:10,000,
619 GE Healthcare) and HRP-linked goat anti-rabbit (1:10,000, GE Healthcare). Antibodies were
620 incubated in 5% non-fat milk PBST (PBS with 0.1% Triton X-100) and washed with PBST.
621 Chemiluminescence detection was performed with the Amersham imager 600 (GE
622 Healthcare).

623 **Mass Spectrometry**

624 Proteins were extracted from the ovaries of 100 3-day-old, well-fed females of each
625 genotype, crossed to wild-type males, and proteins were boiled and run on SDS-PAGE. The
626 gel was then stained with Coomassie Blue. The gel pieces containing the α-tubulin region
627 were cut, alkylated, and digested by trypsin N (ProtiFi) for 3 hours at 55°C. C-terminal
628 peptides of α-tubulin were analyzed by liquid chromatography (LC)-MS/MS (PROXEON
629 coupled to a QExactive mass spectrometer, Thermo Fisher Scientific). Samples were
630 searched against the UniProtKB *Drosophila* database using Pipeline, PEAKS, Easyprot, and
631 MSfragger as search engines. Peptides were identified by PSM value (peptide spectrum
632 match). To avoid repetition of total PSM quantification, we searched only for one type of
633 PTM in an analysis each time. Total PSM indicates the sum of PSMs of primary C-terminal
634 peptides with either glutamylation or glycylation modifications or non-modified peptides.

635 **Ooplasmic streaming in living oocytes**

636 Three days old females were kept together with wild-type males under non-crowding
637 conditions at 25°C on food containing dry yeast. The determination of ooplasmic streaming
638 was based on the method of Lu and colleagues (Lu et al., 2016). Ovaries were directly
639 dissected in 10 S halocarbon oil (VWR), and egg chambers were teased apart in the oil drop
640 on 24×50 mm coverslips (VWR). Living Stage 10B oocytes were directly observed and
641 imaged under the 60×1.4 NA oil immersion objective on a Nikon W1 LIPSI spinning disk with
642 a 2x Photometrics Prime BSI CMOS camera. Time-lapse images were acquired every 2s for
643 2 min under bright-field (BF) controlled by Nikon Elements software. Flow tracks were
644 generated by kymographs using Fiji (Schindelin et al., 2012) plugin Multi Kymograph
645 (HTTPS:// imagej.net/ Multi _Kymograph).

646 **Immunostaining and confocal microscopy**

647 Ovaries were dissected in 1× PBS and fixed in buffer (200 µl 4% formaldehyde (Sigma), 600
648 ul Heptane (Merck Millipore), 20 ul DMSO (Sigma) for each group) for 20 min. Ovaries were
649 then blocked in 2% milk powder in PBST (PBS, 0.5% Triton X-100). Samples were
650 incubated with rabbit anti-Staufen (1:2,000) (St Johnston et al., 1991), mouse anti-Gurken
651 (1D12, 1:10) (Queenan et al., 1999), mouse anti-BicD (1B11 plus 4C2, 1:5) (Suter and
652 Steward, 1991), rabbit anti-Khc (1:150, Cytoskeleton), rabbit anti-GFP (1:200, Sigma) and
653 mouse anti-1D5 (1:150, Synaptic System) at 4°C overnight, and incubated with secondary
654 Alexa Fluor goat anti-mouse Cy3 (1:400, Jackson ImmonoResearch) and Alexa Fluor goat
655 anti-rabbit 488 (1:400, Life technologies Thermo Fischer) at room temperature for 3h. DNA

656 and nuclei were stained using Hoechst 33528 (Thermo Fischer Scientific) for 10 min.
657 Mounted samples were imaged with a Leica TCS SP8 confocal microscope equipped with a
658 63×1.40 oil lens and controlled by the Las X software (Leica). Images of single focal planes
659 and 12 μm Z projection were acquired. The crescent length of Staufen was processed by the
660 Fuji segmented line tool based on a single plane. The data were shown as means ± SEM by
661 Prism 5 (GraphPad software). The statistical significance was determined by an unpaired
662 two-tailed non-parametric t-test (Mann-Whitney test). For the Khc intensity analysis, the
663 intensity of fluorescence in the oocyte was plotted and the intensity charts were generated
664 using Fiji's "Analyze-Plot profile" function.

665 **Mitochondrial transport in *Drosophila* wing neurons**

666 Mitochondrial transport in *Drosophila* wing neurons was tracked as described (Vagnoni and
667 Bullock, 2016). In brief, 1-2 days old flies were anesthetized with CO_2 and immobilized in a
668 custom-built chamber formed of two No.1.5 24×50 mm coverslips (VWR). Imaging of wings
669 was performed with a Nikon W1 LIPSI spinning disk microscope equipped with a 2x
670 Photometrics Prime BSI CMOS camera and a 60×1.4 NA oil immersion lens. Time-lapse
671 video of a single focal plane was acquired with an acquisition rate of 0.5 frame/s for 3 min for
672 Mito::GFP using a 488 nm laser.

673 Quantification of the movements was performed in Fiji. At least 7 wings of each genotype
674 were tracked for quantification. A region of the wing arch of the L1 vein was selected and
675 straightened with the Straighten plugin (Eva Kocsis, NIH, MD). For each "run", the total
676 trafficking distance of more than 2 μm was defined as "motile mitochondria". To exclude the
677 oscillatory movements of mitochondria, a minimal instant velocity between each frame was
678 defined at 0.2 μm/s. Transported mitochondria were manually tracked by the manual
679 tracking plugin (Fabrice Cordelières, Institute Curie, France). Kymographs of individual
680 mitochondria were produced using Fiji (Schindelin et al., 2012) plugin Multi Kymograph
681 (HTTPS:// imagej.net/ Multi _Kymograph). Run length, instant velocity values, and total
682 running, trafficking & pausing times were exported into Excel for analysis. The data are
683 shown as means ± SEM by Prism 5 (GraphPad). The statistical significance was determined
684 with the student's t-test.

685 **Sequence alignment**

686 Sequences were aligned by CLC Sequence Viewer 8.0 software (Qiagen). The UniProtKB
687 accession numbers are as follows: *HsTTL*: Q8NG68; *HsTTLL5*: Q6EMB2; *MmTTLL5*:
688 Q8CHB8; *DmTTLL5*: Q9VBX5;

Acknowledgments

We thank Simon L. Bullock (Cambridge, UK) for *ApplGal4* and *UAS-mito::GFP* fly lines, Michel Steinmetz (Paul Scherrer Institute, Switzerland), and the Carsten Janke (Institute Curie, France) laboratory members for discussions and suggestions. We also thank the University of Bern (Switzerland) Mass Spectrometry center members Sophie Braga Lagache and Natasha Buchs for performing the MS experiments and Manfred Heller and Anne-Christine Uldry for peptide analysis and discussion of the results.

Support

This work was financially supported by the project grants 31003A_173188 and 310030_205075 from the Swiss National Science Foundation (SNF; https://www.snf.ch/en) to BS. Equipment support was by an equipment grant from SNF (316030_150824) to BS and by the University of Bern (https://www.unibe.ch). Additional salary and material support were received from the University of Bern (https://www.unibe.ch) to BS. The funders had no role in the study design, data collection, analysis, decision to publish, or manuscript preparation.

The authors declare no competing financial interests.

Author contributions: Mengjing Bao, Beat Suter, and Maria Paula Vazquez-Pianzola conceived the project and designed the experiments. Mengjing Bao, Beat Suter, Ruth Dörig, and Dirk Beuchle performed the experiments and analyzed the data; Mengjing Bao and Beat Suter wrote the manuscript.

Reference

Arce, C.A., J.A. Rodriguez, H.S. Barra, and R. Caputo. 1975. Incorporation of L-tyrosine, L-phenylalanine, and L-3,4-dihydroxyphenylalanine as single units into rat brain tubulin. *Eur J Biochem*. 59:145-149.

Bodakuntla, S., A. Schnitzler, C. Villablanca, C. Gonzalez-Billault, I. Bieche, C. Janke, and M.M. Magiera. 2020. Tubulin polyglutamylation is a general traffic-control mechanism in hippocampal neurons. *J Cell Sci*. 133.

Bodakuntla, S., X. Yuan, M. Genova, S. Gadadhar, S. Leboucher, M.C. Birling, D. Klein, R. Martini, C. Janke, and M.M. Magiera. 2021. Distinct roles of α- and β-tubulin polyglutamylation in controlling axonal transport and in neurodegeneration. *EMBO J*. 40:e108498.

722 Bré, M.H., V. Redeker, M. Quibell, J. Darmanaden-Delorme, C. Bressac, J. Cosson, P.
723 Huitorel, J.M. Schmitter, J. Rossler, T. Johnson, A. Adoutte, and N. Levilliers. 1996.
724 Axonemal tubulin polyglycylation probed with two monoclonal antibodies: widespread
725 evolutionary distribution, appearance during spermatozoan maturation and possible
726 function in motility. *J Cell Sci*. 109 (Pt 4):727-738.
727 Brendza, R.P., L.R. Serbus, J.B. Duffy, and W.M. Saxton. 2000. A function for kinesin I in
728 the posterior transport of oskar mRNA and Staufen protein. *Science*. 289:2120-2122.
729 Claussen, M., and B. Suter. 2005. BicD-dependent localization processes: from Drosophila
730 development to human cell biology. *Ann Anat*. 187:539-553.
731 Devambez, I., J. van Dijk, S. Benlefki, S. Layalle, Y. Grau, K. Rogowski, M.L. Parmentier,
732 and L. Soustelle. 2017. Identification of DmTTLL5 as a Major Tubulin Glutamylase in
733 the Drosophila Nervous System. *Sci Rep*. 7:16254.
734 Díaz-Valencia, J.D., M.M. Morelli, M. Bailey, D. Zhang, D.J. Sharp, and J.L. Ross. 2011.
735 Drosophila katanin-60 depolymerizes and severs at microtubule defects. *Biophys J*.
736 100:2440-2449.
737 Eddé, B., J. Rossier, J.P. Le Caer, E. Desbruyères, F. Gros, and P. Denoulet. 1990.
738 Posttranslational glutamylation of alpha-tubulin. *Science*. 247:83-85.
739 Gadadhar, S., G. Alvarez Viar, J.N. Hansen, A. Gong, A. Kostarev, C. Ialy-Radio, S.
740 Leboucher, M. Whitfield, A. Ziyyat, A. Touré, L. Alvarez, G. Pigino, and C. Janke.
741 2021. Tubulin glycylation controls axonemal dynein activity, flagellar beat, and male
742 fertility. *Science*. 371.
743 Gadadhar, S., S. Bodakuntla, K. Natarajan, and C. Janke. 2017. The tubulin code at a
744 glance. *J Cell Sci*. 130:1347-1353.
745 Genova, M., L. Grycova, V. Puttrich, M.M. Magiera, Z. Lansky, C. Janke, and M. Braun.
746 2023. Tubulin polyglutamylation differentially regulates microtubule-interacting
747 proteins. *EMBO J*:e112101.
748 Hallak, M.E., J.A. Rodriguez, H.S. Barra, and R. Caputto. 1977. Release of tyrosine from
749 tyrosinated tubulin. Some common factors that affect this process and the assembly
750 of tubulin. *FEBS Lett*. 73:147-150.
751 Heerssen, H., R.D. Fetter, and G.W. Davis. 2008. Clathrin dependence of synaptic-vesicle
752 formation at the Drosophila neuromuscular junction. *Curr Biol*. 18:401-409.
753 Hollenbeck, P.J., and W.M. Saxton. 2005. The axonal transport of mitochondria. *J Cell Sci*.
754 118:5411-5419.
755 Janke, C., K. Rogowski, D. Wloga, C. Regnard, A.V. Kajava, J.M. Strub, N. Temurak, J. van
756 Dijk, D. Boucher, A. van Dorsselaer, S. Suryavanshi, J. Gaertig, and B. Eddé. 2005.
757 Tubulin polyglutamylase enzymes are members of the TTL domain protein family.
758 *Science*. 308:1758-1762.
759 Kalfayan, L., and P.C. Wensink. 1982. Developmental regulation of Drosophila alpha-tubulin
760 genes. *Cell*. 29:91-98.
761 Kato, Y., and A. Nakamura. 2012. Roles of cytoplasmic RNP granules in intracellular RNA
762 localization and translational control in the Drosophila oocyte. *Dev Growth Differ*.
763 54:19-31.
764 Kim, M.S., J. Zhong, and A. Pandey. 2016. Common errors in mass spectrometry-based
765 analysis of post-translational modifications. *Proteomics*. 16:700-714.
766 L'Hernault, S.W., and J.L. Rosenbaum. 1985. Chlamydomonas alpha-tubulin is
767 posttranslationally modified by acetylation on the epsilon-amino group of a lysine.
768 *Biochemistry*. 24:473-478.
769 Lee, G.S., Y. He, E.J. Dougherty, M. Jimenez-Movilla, M. Avella, S. Grullon, D.S. Sharlin, C.
770 Guo, J.A. Blackford, Jr., S. Awasthi, Z. Zhang, S.P. Armstrong, E.C. London, W.
771 Chen, J. Dean, and S.S. Simons, Jr. 2013. Disruption of Ttll5/stamp gene (tubulin
772 tyrosine ligase-like protein 5/SRC-1 and TIF2-associated modulatory protein gene) in
773 male mice causes sperm malformation and infertility. *J Biol Chem*. 288:15167-15180.
774 Lu, W., M. Lakonishok, A.S. Serpinskaya, D. Kirchenbüechler, S.C. Ling, and V.I. Gelfand.
775 2018. Ooplasmic flow cooperates with transport and anchorage in. *J Cell Biol*.
776 217:3497-3511.

Lu, W., M. Winding, M. Lakonishok, J. Wildonger, and V.I. Gelfand. 2016. Microtubule-microtubule sliding by kinesin-1 is essential for normal cytoplasmic streaming in Drosophila oocytes. *Proc Natl Acad Sci U S A*. 113:E4995-5004.

Magiera, M.M., and C. Janke. 2014. Post-translational modifications of tubulin. *Curr Biol*. 24:R351-354.

Mahalingan, K.K., E. Keith Keenan, M. Strickland, Y. Li, Y. Liu, H.L. Ball, M.E. Tanner, N. Tjandra, and A. Roll-Mecak. 2020. Structural basis for polyglutamate chain initiation and elongation by TTLL family enzymes. *Nat Struct Mol Biol*. 27:802-813.

Mao, C.X., Y. Xiong, Z. Xiong, Q. Wang, Y.Q. Zhang, and S. Jin. 2014. Microtubule-severing protein Katanin regulates neuromuscular junction development and dendritic elaboration in Drosophila. *Development*. 141:1064-1074.

McKenney, R.J., W. Huynh, R.D. Vale, and M. Sirajuddin. 2016. Tyrosination of α-tubulin controls the initiation of processive dynein-dynactin motility. *Embo j*. 35:1175-1185.

Monteith, C.E., M.E. Brunner, I. Djagaeva, A.M. Bielecki, J.M. Deutsch, and W.M. Saxton. 2016. A Mechanism for Cytoplasmic Streaming: Kinesin-Driven Alignment of Microtubules and Fast Fluid Flows. *Biophys J*. 110:2053-2065.

Natarajan, K., S. Gadadhar, J. Souphron, M.M. Magiera, and C. Janke. 2017. Molecular interactions between tubulin tails and glutamylases reveal determinants of glutamylation patterns. *EMBO Rep*. 18:1013-1026.

Neuman-Silberberg, F.S., and T. Schüpbach. 1996. The Drosophila TGF-alpha-like protein Gurken: expression and cellular localization during Drosophila oogenesis. *Mech Dev*. 59:105-113.

Pilling, A.D., D. Horiuchi, C.M. Lively, and W.M. Saxton. 2006. Kinesin-1 and dynein are the primary motors for fast transport of mitochondria in Drosophila motor axons. *Mol Biol Cell*. 17:2057-2068.

Port, F., H.M. Chen, T. Lee, and S.L. Bullock. 2014. Optimized CRISPR/Cas tools for efficient germline and somatic genome engineering in Drosophila. *Proc Natl Acad Sci U S A*. 111:E2967-2976.

Preston, S.F., G.G. Deanin, R.K. Hanson, and M.W. Gordon. 1979. The phylogenetic distribution of tubulin:tyrosine ligase. *J Mol Evol*. 13:233-244.

Prota, A.E., M.M. Magiera, M. Kuijpers, K. Bargsten, D. Frey, M. Wieser, R. Jaussi, C.C. Hoogenraad, R.A. Kammerer, C. Janke, and M.O. Steinmetz. 2013. Structural basis of tubulin tyrosination by tubulin tyrosine ligase. *J Cell Biol*. 200:259-270.

Queenan, A.M., G. Barcelo, C. Van Buskirk, and T. Schüpbach. 1999. The transmembrane region of Gurken is not required for biological activity, but is necessary for transport to the oocyte membrane in Drosophila. *Mech Dev*. 89:35-42.

Redeker, V., N. Levilliers, J.M. Schmitter, J.P. Le Caer, J. Rossier, A. Adoutte, and M.H. Bré. 1994. Polyglycylation of tubulin: a post-translational modification in axonemal microtubules. *Science*. 266:1688-1691.

Redeker, V., R. Melki, D. Promé, J.P. Le Caer, and J. Rossier. 1992. Structure of tubulin C-terminal domain obtained by subtilisin treatment. The major alpha and beta tubulin isotypes from pig brain are glutamylated. *FEBS Lett*. 313:185-192.

Rogowski, K., F. Juge, J. van Dijk, D. Wloga, J.M. Strub, N. Levilliers, D. Thomas, M.H. Bré, A. Van Dorsselaer, J. Gaertig, and C. Janke. 2009. Evolutionary divergence of enzymatic mechanisms for post-translational polyglycylation. *Cell*. 137:1076-1087.

Rogowski, K., J. van Dijk, M.M. Magiera, C. Bosc, J.C. Deloulme, A. Bosson, L. Peris, N.D. Gold, B. Lacroix, M. Bosch Grau, N. Bec, C. Larroque, S. Desagher, M. Holzer, A. Andrieux, M.J. Moutin, and C. Janke. 2010. A family of protein-deglutamylating enzymes associated with neurodegeneration. *Cell*. 143:564-578.

Rüdiger, A.H., M. Rüdiger, J. Wehland, and K. Weber. 1999. Monoclonal antibody ID5: epitope characterization and minimal requirements for the recognition of polyglutamylated alpha- and beta-tubulin. *Eur J Cell Biol*. 78:15-20.

Schindelin, J., I. Arganda-Carreras, E. Frise, V. Kaynig, M. Longair, T. Pietzsch, S. Preibisch, C. Rueden, S. Saalfeld, B. Schmid, J.Y. Tinevez, D.J. White, V.

831 Hartenstein, K. Eliceiri, P. Tomancak, and A. Cardona. 2012. Fiji: an open-source
832 platform for biological-image analysis. *Nat Methods*. 9:676-682.
833 Serbus, L.R., B.J. Cha, W.E. Theurkauf, and W.M. Saxton. 2005. Dynein and the actin
834 cytoskeleton control kinesin-driven cytoplasmic streaming in Drosophila oocytes.
835 *Development*. 132:3743-3752.
836 Sherwood, N.T., Q. Sun, M. Xue, B. Zhang, and K. Zinn. 2004. Drosophila spastin regulates synaptic
837 microtubule networks and is required for normal motor function. *PLoS Biol*. 2:e429
838 Sirajuddin, M., L.M. Rice, and R.D. Vale. 2014. Regulation of microtubule motors by tubulin
839 isotypes and post-translational modifications. *Nat Cell Biol*. 16:335-344.
840 Skiniotis, G., J.C. Cochran, J. Müller, E. Mandelkow, S.P. Gilbert, and A. Hoenger. 2004.
841 Modulation of kinesin binding by the C-termini of tubulin. *EMBO J*. 23:989-999
842 St Johnston, D., D. Beuchle, and C. Nüsslein-Volhard. 1991. Staufen, a gene required to
843 localize maternal RNAs in the Drosophila egg. *Cell*. 66:51-63.
844 Suter, B. 2018. RNA localization and transport. *Biochim Biophys Acta Gene Regul Mech*.
845 1861:938-951.
846 Suter, B., and R. Steward. 1991. Requirement for phosphorylation and localization of the
847 Bicaudal-D protein in Drosophila oocyte differentiation. *Cell*. 67:917-926.
848 Szczesna, E., E.A. Zehr, S.W. Cummings, A. Szyk, K.K. Mahalingan, Y. Li, and A. Roll-
849 Mecak. 2022. Combinatorial and antagonistic effects of tubulin glutamylation and
850 glycylation on katanin microtubule severing. *Dev Cell*. 57:2497-2513.e2496.
851 Theurkauf, W.E., H. Baum, J. Bo, and P.C. Wensink. 1986. Tissue-specific and constitutive
852 alpha-tubulin genes of Drosophila melanogaster code for structurally distinct proteins.
853 *Proc Natl Acad Sci U S A*. 83:8477-8481.
854 Trotta, N., G. Orso, M.G. Rossetto, A. Daga, and K. Broadie. 2004. The hereditary spastic paraplegia
855 gene, spastin, regulates microtubule stability to modulate synaptic structure and
856 function. *Curr Biol*. 14:1135-1147.
857 Vagnoni, A., and S.L. Bullock. 2016. A simple method for imaging axonal transport in aging
858 neurons using the adult Drosophila wing. *Nat Protoc*. 11:1711-1723.
859 Valenstein, M.L., and A. Roll-Mecak. 2016. Graded Control of Microtubule Severing by
860 Tubulin Glutamylation. *Cell*. 164:911-921.
861 van Dijk, J., K. Rogowski, J. Miro, B. Lacroix, B. Eddé, and C. Janke. 2007. A targeted
862 multienzyme mechanism for selective microtubule polyglutamylation. *Mol Cell*.
863 26:437-448.
864 Weil, T.T. 2014. mRNA localization in the Drosophila germline. *RNA Biol*. 11:1010-1018.
865 Wolff, A., B. de Néchaud, D. Chillet, H. Mazarguil, E. Desbruyères, S. Audebert, B. Eddé, F.
866 Gros, and P. Denoulet. 1992. Distribution of glutamylated alpha and beta-tubulin in
867 mouse tissues using a specific monoclonal antibody, GT335. *Eur J Cell Biol*. 59:425-
868 432.
869 Zimyanin, V., N. Lowe, and D. St Johnston. 2007. An oskar-dependent positive feedback
870 loop maintains the polarity of the Drosophila oocyte. *Curr Biol*. 17:353-359.
871 Zimyanin, V.L., K. Belaya, J. Pecreaux, M.J. Gilchrist, A. Clark, I. Davis, and D. St Johnston.
872 2008. In vivo imaging of oskar mRNA transport reveals the mechanism of posterior
873 localization. *Cell*. 134:843-853.
874

875

876

877 **Table 1) Conservation between mammalian TTLL5 and *Drosophila* TTLL5**

878 Residues labeled in red are critical residues for α-tubulin glutamylation by murine TTLL5 and are
879 conserved in human and *Drosophila* TTLL5 (van Dijk et al., 2007, Natarajan et al., 2017).

	K131 β6-7 loop (R188) R225 E366 N368
Mm TTLL5	TRKDR—KPVASSRGRG[1)]VY---VRLYVL---LLEVNLSP
Hs TTLL5	TRKDR—KPVASSRGRG VY---VRLYVL---LLEVNLSP
	K282 β6-7 loop (R339) R376 E517 N519
Dm TTLL5	TRKDR--KPAASSRGRG I F---LRVYVL---LLEI NLSP

880 [1)] The critical domain of the β6-7 loop is highlighted with a yellow background.

881

882 **Table 2) Role of *TTLL5* for the glutamylation of the C-terminal domain of αTub84B/D.**
883 Frequency of glutamylated C-terminal peptides (containing the entire primary sequence) in *w* controls,
884 *TTLL5*^{pBac,} and *TTLL5*^{MiEx} mutants containing modifications of 1E, 2E, or 3Es.

	w[1)]	*TTLL5*^{pBac} (*%E mod*)	*TTLL5*^{MiEx}
+1	41	0	0
+2	14	0	0
+3	7	0	0
Total Glu modifications[2)]	62	0	0

885 [1)] The total peptide numbers (n) were indicated by the values of total PSM (peptide spectrum match) of the full
886 primary C-terminal αTub84B/D sequence. The n for *w*, *TTLL5*^{pBac}, and *TTLL5*^{MiEx} were 56, 29, and 7,
887 respectively.
888 [2)] Total Glu modifications show the sum of the three frequencies. The ratio was quantified based on the
889 glutamylated C-terminal αTub84B/D PSM values divided by total PSM.

890

891 **Table 3) Conservation between TTL and TTLL5**

892 Many critical residues of human TTL (red) are conserved in *Drosophila,* mouse, and human TTLL5
893 (Prota et al., 2013).

	R202 R222 D318 E331 N333 P336
Hs TTL	IRSW—VLRTA-----FDFM—LI EVNGAPA
	R376 R398 D504 E517 N519 P522
Dm TTLL5	LRVY---I VRLA-----FDIL----LLEI NL SPS
	R225 R247 D353 E366 N368 P371
Mm TTLL5	VRLY---LARFA-----FDVL---LLEVNL SPS
	R225 R247 D353 E366 N368 P371
Hs TTLL5	VRLY---LARFA-----FDVL---LLEVNL SPS

894

895

896 **Figure legends**

897 **Fig. 1 Mass spectrometry analysis of glutamylation of the C-terminal domains of**
898 ***Drosophila* α-tubulins.** A) Schematic representation showing how the C-terminal regions of
899 αTub84B/D can be modified by glutamic acid residues added to the side chains of E443,
900 E445, E448, and E449 in *Drosophila* ovaries. B) The C-terminal peptides containing the
901 complete primary sequence were analyzed. The structure of the different C-terminal tail
902 peptides of αTub84B/D modified by glutamylation is shown starting with G442. Different
903 combinations of Glu side chain modifications were found added at positions E443, E445,
904 E448, and E449 of αTub84B/D. Schemes were drawn by biorender.com.

905 **Fig. 2 Schematic representation of the *Drosophila TTLL5* gene, *TTLL5*^{pBac}, *TTLL5*^{MiEx},**
906 **and Venus::TTLL5 proteins.** A) The *TTLL5* gene structure is based on the FlyBase data for
907 the *CG31108-RA* transcript. The positions of the loss-of-function mutations are marked on
908 the *TTLL5* gene. Grey triangles: transposon insertions. Grey asterisks: codons targeted for
909 generating InDels and point mutations. All *TTLL5* alleles were analyzed as hemizygous
910 animals over *Df(3R)BSC679*, which removes the region of the *TTLL5* gene. B) Western blot
911 from the soluble fraction of ovarian extracts. *w* (*TTLL5*$^{+}$/$^{+}$*),* which contains two wild-type
912 copies of *TTLL5*, expressed the highest levels of TTLL5. The TTLL5 signal is strongly
913 reduced or abolished in the null mutants *TTLL5*^{pBac}/$^{-}$*, TTLL5*^{Mi}/$^{-}$, and *TTLL5*^{MiEx}/$^{-}$ compared to
914 *w.* The hemizygous *TTLL5*$^{+}$ ovaries (*TTLL5*$^{+}$/$^{-}$) expressed less TTLL5 than *w.* The signal of
915 an unspecific band (labeled with *), produced after a short exposure, was used as the
916 loading control. In the following, we will refer to the genotypes as *w* for the control (*TTLL5*$^{+}$/$^{+}$)
917 and *TTLL5*^{allele} for the hemizygous mutants *(TTLL5*^{allele}/$^{-}$).

918 **Fig. 3 *TTLL5* is required for the glutamylation of α-tubulin in ovaries.** A), C) Sites on
919 αTub84B/D expected to be recognized by the antibody against monoglutamylated α-Tubulin
920 (GT335; A) and by the 1D5 antibody recognizing polyglutamylated αTub (C). B), D) The
921 glutamylation signal, produced by Western blotting with the GT335 and 1D5 antibodies,
922 respectively, is lower in *TTLL5*^{pBac}*, TTLL5*^{Mi}, and *TTLL5*^{MiEx} than in the *w* control but is
923 restored and even elevated in mutant ovaries that express *Venus::TTLL5* under *MattubGal4*
924 control. The up-shifted bands recognized by 1D5 can be seen in the rescued *TTLL5*^{pBac} and
925 *TTLL5*^{Mi} mutants. The total tyrosinated α-tubulin levels seemed unaffected by the TTLL5
926 levels. α-tubulin and GAPDH served as loading controls. E) The genotypes and rationale of
927 the *TTLL5* alleles generated by CRISPR/Cas9 are listed. The selected residues are
928 predicted to be either important for the glutamylation or tyrosination function based on the
929 alignment shown in **Tables 3** and **4**. F) Western blotting shows that the polyglutamylation

930 signal is absent in all point mutants. *w* with two copies of *TTLL5*$^{+}$ is the wild-type control and
931 the hemizygous *TTLL5*$^{TRK282>KGK282}$ still contains the crucial K282 residue and behaves like
932 the control. Relative to the loading controls, 1D5 signals decrease slightly in the hemizygous
933 situation with only one *TTLL5*$^{+}$ copy. G) Stronger up-shifted bands were observed with the
934 polyglutamylation antibody (1D5) upon *Venus::TTLL5* overexpression in wild-type
935 ovaries. Total α-tubulin levels were similar in samples with excessive expression of *TTLL5.*
936 GAPDH was a loading control. All mutant *TTLL5* alleles were analyzed as hemizygous
937 animals over *Df(3R)BSC679*. The genotypes of the rescued animals were *MattubGal4>UAS-*
938 *Venus::TTLL5;TTLL5*^{alleles}*/Df(3R)BSC679.* The genotype of the *Venus::TTLL5*
939 overexpressing animals was *MattubGal4>UAS-Venus::TTLL5.*

940 **Fig. 4 Spatial distribution of polyglutamylated microtubules in the oocyte.** Confocal
941 micrographs showing representative oocytes and follicle cells from early to late stages of *w*
942 controls and *TTLL5*^{MiEx} mutants. Polyglutamylation (1D5) signals are shown in magenta and
943 Hoechest (blue) stains the DNA. A 1D5 signal is seen in follicle cells and oocytes from
944 previtellogenic to late-stage oocytes. For the S10B oocytes, a high-power magnification of
945 the posterior half is shown, too. At this stage, a slightly biased 1D5 signal intensity was seen
946 in the cortical region of the oocyte (marked by white arrowheads). The 1D5 signal is virtually
947 absent in the *TTLL5* mutants. Imaging conditions and confocal microscope settings were
948 identical for the two genotypes. The genotype of the control was *w.* Genotypes for *TTLL5*^{MiEx}
949 were *TTLL5*^{MiEx}*/Df(3R)BSC679*.

950 **Fig. 5 Effect of *TTLL5* on Staufen localization refinement in oocytes.** A)-D) Confocal
951 micrographs showing S10B oocytes of *w* controls (A), *TTLL5*^{pBac}*, TTLL5*^{Mi}, and *TTLL5*^{MiEx}
952 mutants (B), *TTLL5*^{pBac}*, TTLL5*^{Mi}, and *TTLL5*^{MiEx} mutants rescued by *Mattub4>UASP-*
953 *Venus::TTLL5* (C), *TTLL5*^{E517A}*, TTLL5*^{P522A}*,* and *TTLL5*^{R339A} mutants (D). Anti-Staufen is
954 shown in green, anti-GFP in red, and Hoechst (DNA) in blue. E) Quantification of the Staufen
955 crescent length along the posterior cortex based on A-D) *** $p<0.005$. z-stack: 12µm. F)
956 Confocal micrographs showing previtellogenic and S9 egg chambers of *w* controls,
957 *TTLL5*^{pBac}*, TTLL5*^{MiEx}*,* and *TTLL5*^{E517A} mutants. Staufen signal is shown in green, and
958 Hoechst in blue. Scale Bar: 25µm. *TTLL5*^{MiEx} and *TTLL5*^{E517A} were hemizygous over
959 *Df(3R)BSC679*. The genotype for *TTLL5*^{pBac} was *MattubGal4/+; TTLL5*^{pBac}*/Df(3R)BSC679.*
960 The genotypes of the rescued animals were *MattubGal4/UASP-Venus::TTLL5; TTLL5*
961 ^{alleles}*/Df(3R)BSC679.*

962 **Fig. 6 Role of *TTLL5* in fast ooplasmic streaming.** A) Example of an S10B oocyte used
963 for particle flow measurements based on time-lapse movies of ooplasmic streaming

964 (**Mov.S1-S5**). Scale Bar: 25 µm. B) Kymographs were generated along a line close to the
965 posterior cortex on one side of the ooplasm (region marked by a yellow line in A). Sample
966 kymographs were shown based on the **Movie S1-S5**. Streaming was shown from 2
967 representative oocytes for each movie. The first and second oocytes are marked as sample
968 1 (#1) and sample 2 (#2), respectively. The unidirectional streaming along the posterior
969 cortex is seen in the two control and the *TTLL5* rescue samples, and in sample 1 of the
970 *TTLL5* overexpressing oocyte. Disordered streaming is seen in the second sample of the
971 *TTLL5* overexpressing line and both samples of the *TTLL5* mutants. C) Quantification of
972 streaming patterns seen in the different genotypes. 100% control (n=17), 71%*TTLL5*
973 rescued (n=7) and 71% *TTLL5* overexpression (n=21) S10B oocytes showed an overall
974 circular unidirectional streaming pattern. In contrast, 76% $TTLL5^{MiEx}$ (n=21) and 100%
975 $TTLL5^{E517A}$ (n=10) oocytes showed an abnormal streaming pattern. The stronger penetrance
976 of the $TTLL5^{E517A}$ phenotype (C) compared to the null mutant could be seen as evidence for
977 a slight dominant effect of the point mutation. This is consistent with the stronger expressivity
978 of the streaming defects observed in the movies (B, D), although the numbers appear a bit
979 small to firmly conclude this. D) Schematic representation of the different streaming patterns
980 observed. The frequency with which each streaming pattern was observed in the different
981 genotypes is indicated from high (left) to low (right). “Circular streaming pattern” was further
982 subdivided into “central streaming pattern (top)” and “anterior-biased streaming pattern
983 (below)”. The “central streaming” was observed in all controls, 71% of the *TTLL5* rescue,
984 43% of the *TTLL5* overexpression, and 21% of the $TTLL5^{MiEx}$ oocytes. The “anterior-biased
985 streaming” was frequently seen in 28% of the *TTLL5* overexpression ovaries, where the
986 main circular center moved to the anterior part, leaving the posterior with a chaotic streaming
987 flow. “Abnormal streaming” included the oocytes that showed an overall chaotic flow
988 direction (upper one) and the partially disrupted flow (below). The abnormal streaming
989 patterns were mainly seen in the situations when *TTLL5* was insufficient or inactive, and at a
990 low frequency also in *TTLL5* rescued and *TTLL5* overexpressing ovaries. The genotype of
991 the control was *w* or *+/Df(3R)BSC679.* The genotypes for $TTLL5^{MiEx}$ and $TTLL5^{E517A}$ were
992 both over *Df(3R)BSC679*. The genotype of the rescued flies was *MattubGal4/UAS-*
993 *Venus::TTLL5;* $TTLL5^{MiEx}$*/Df(3R)BSC679.* The genotype of *TTLL5* overexpressing flies was
994 *MattubGal4/UAS-Venus::TTLL5.*

995 **Fig. 7 Role of *TTLL5* for kinesin distribution in ovaries** A), B) Khc levels remained
996 unchanged between *w* control, *TTLL5* deficient mutants, rescued *TTLL5* mutants, and *TTLL5*
997 overexpressing ovaries. Anti-GFP antibodies reveal the expression of *Venus:TTLL5.*
998 GAPDH served as the loading control. C) E) Confocal micrographs showing the Khc
999 distribution in stage 10B oocytes. C) White arrowheads point to the posterior enrichment of

1000 Khc along the cortical region in the wild-type control and TTLL5 overexpressing oocytes. D)
1001 Blind quantification of the posterior enrichment of Khc. The frequency of oocytes with
1002 posterior enrichment is shown graphically and numerically. n= number of oocytes evaluated.
1003 E) A white line was drawn along the anterior-posterior axis of the oocyte using Fiji. The lines
1004 start at the nurse cell oocyte border on the left and end at the posterior follicle cells. The line
1005 width was 50 units. G) Intensity charts were plotted based on the line drawn along the AP
1006 axis in E). The orange arrowheads in the oocytes and the intensity charts point to the
1007 regions showing higher Khc accumulation in the inner region of the oocyte. F) Fraction of the
1008 oocytes that showed inner hyperaccumulation of Khc were quantified. n= number of oocytes
1009 evaluated. The percentage of oocytes showing inner enrichment of Khc is shown graphically
1010 and numerically. Judging Khc distribution was done blindly by two persons. The fractions
1011 were taken from the mean values obtained from the two persons. Scale Bar: 25μm. The Khc
1012 signal is shown in green, and Hoechst in blue. The genotype for controls was *w* or
1013 *+/Df(3R)BSC679.* Genotype for *TTLL5*^{pBac}: *MattubGal4/+, TTLL5*^{pBac}*/Df(3R)BSC679*;
1014 *TTLL5*^{MiEx}*: TTLL5*^{MiEx}*/Df(3R)BSC679*. Genotype for *TTLL5* overexpression:
1015 *MattubGal4/UAS-Venus::TTLL5.*

1016 **Fig. 8 Role of *TTLL5* in the transport of mitochondria in the L1 wing nerve.** A)
1017 Representative still image of GFP-labelled mitochondria in axons of the L1 vein of both
1018 control and *TTLL5*^{E517A} wings. The position of the L1 region is indicated in the picture above.
1019 B) Scheme of the transport behavior of the mitochondria in the wing neuron. See the main
1020 text for a detailed description. The schema was drawn by biorender.com. C-F) Mean values
1021 of run length, net velocity, trafficking velocity, and pausing time ratio in the control and the
1022 *TTLL5* ^{E517A} mutant for both anterograde and retrograde transport. C) The run length is the
1023 sum of the distances traveled by individual mitochondria in a trafficking state. D) The net
1024 velocity indicates the run distance divided by the run time. The run time is the sum of the
1025 total pausing time plus the total trafficking time. E) Trafficking velocity indicates the mean of
1026 the instant velocity of the trafficking mitochondria. F) The pausing time ratio was calculated
1027 as total pausing time divided by run time. The total pausing time was the sum of the time
1028 when the mitochondria were pausing. G) Kymographs were generated from 3 representative
1029 mitochondria in the control and the *TTLL5*^{E517A} mutant. Yellow arrowheads indicate the
1030 pauses of selected mitochondria over the 3 min time window. H) The mean values of
1031 pausing frequency. Pausing frequency indicates the number of pauses divided by run length.
1032 Mitochondria were quantified from 7 control fly wings and 8 *TTLL5*^{E517A} fly wings. The
1033 numbers of mitochondria (n) analyzed for the anterograde control, anterograde *TTLL5*^{E517A},
1034 retrograde control, and retrograde *TTLL5*^{E517A} were 46, 36, 25, and 21, respectively. ***
1035 $p<0.005$, ** $p<0.01$. Genotypes for controls were a mixture of *ApplGal4;UAS-*

1036 *Mito::GFP;+/Df(3R)BSC679* and *ApplGal4;UAS-Mito::GFP;TTLL5* ^{E517A}/+**.** Genotypes for
1037 *TTLL5*^{E517A} mutants were *ApplGal4; UAS-Mito::GFP; TTLL5*^{E517A}*/Df(3R)BSC679***.**

Fig. 1

A **α-tubulin isotypes in *Drosophila* ovaries**

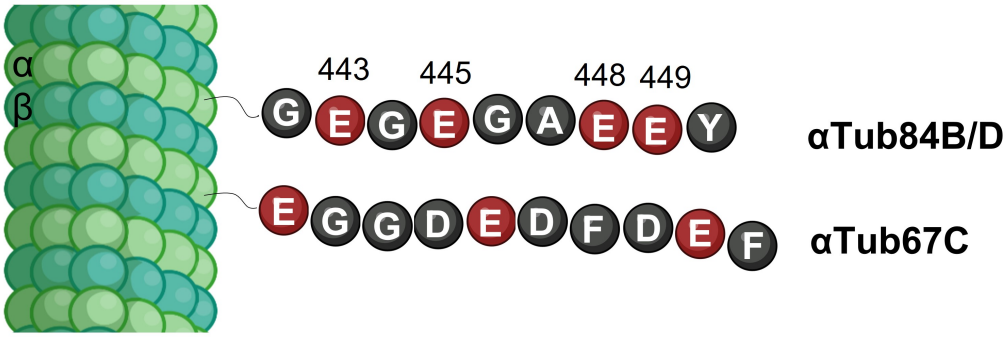

E-residues were found added at the αTub84B/D positions E443, E445, E448 and E449.

B **Glutamylation on E residues in the C-terminal domain of αTub84B/D**

GEGEGAEEY E	GEGEGAEEY E	GEGEGAEEY E	GEGEGAEEY E
GEGEGAEEY EE	GEGEGAEEY EE	GEGEGAEEY EE	GEGEGAEEY EE
GEGEGAEEY EEE	GEGEGAEEY EEE	GEGEGAEEY EEE	GEGEGAEEY EEE
GEGEGAEEY E E	GEGEGAEEY E EE	GEGEGAEEY E E	GEGEGAEEY E EE
GEGEGAEEY EEE	GEGEGAEEY E E E		

Fig. 2

A

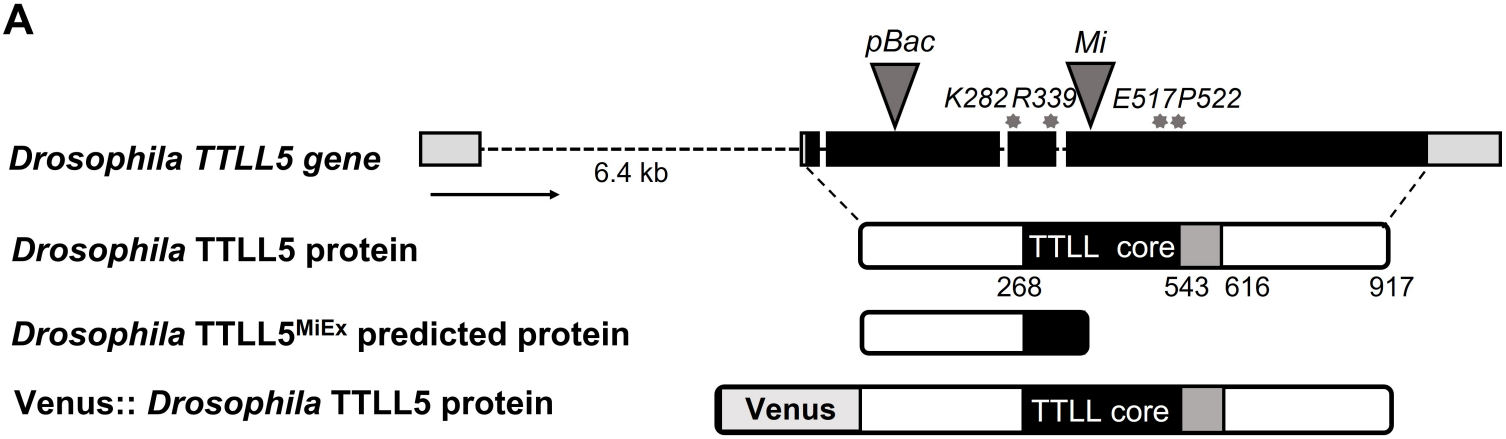
pBac
Mi
K282 R339
E517 P522
Drosophila TTLL5 gene
6.4 kb
Drosophila TTLL5 protein
TTLL core
268
543 616
917
Drosophila TTLL5MiEx predicted protein
Venus:: Drosophila TTLL5 protein
Venus
TTLL core

B

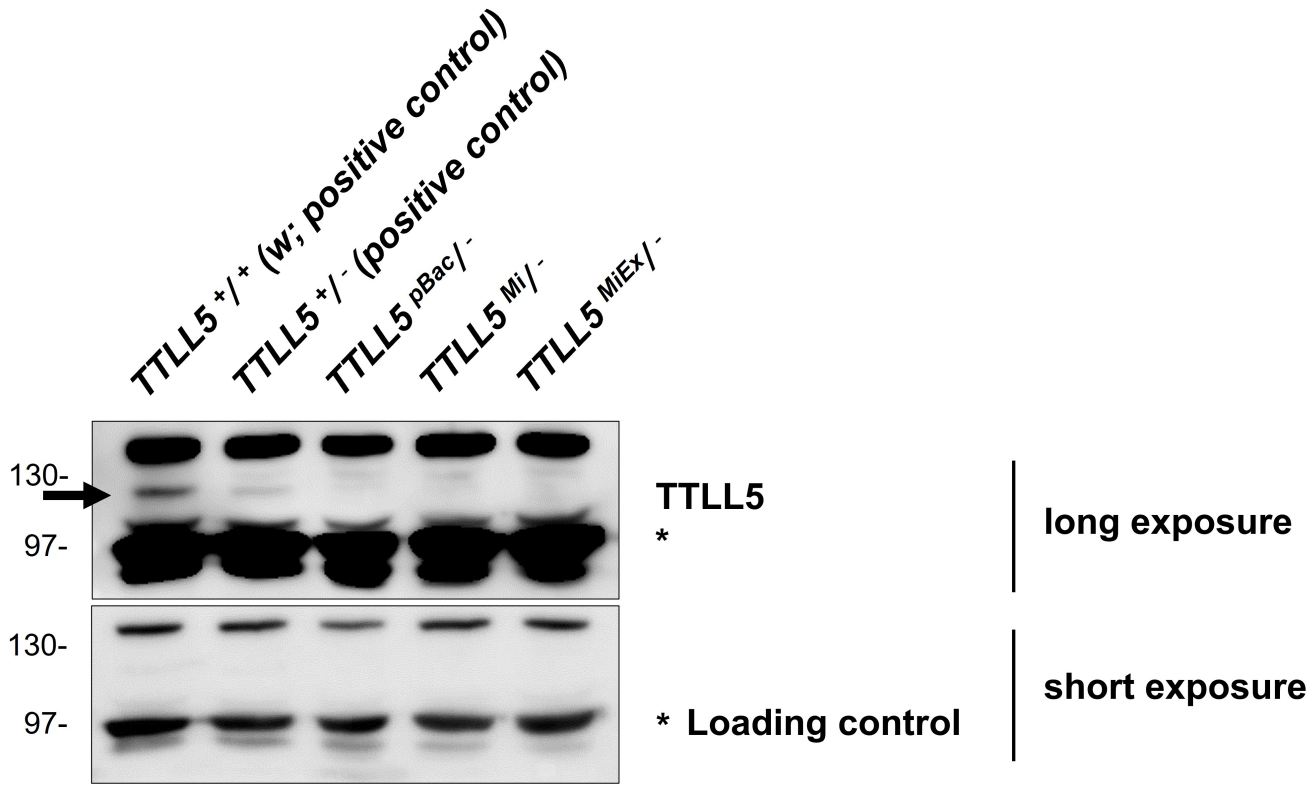
TTLL5 +/+ (w; positive control)
TTLL5 +/- (positive control)
TTLL5 pBac/-
TTLL5 Mi/-
TTLL5 MiEx/-
130-
97-
TTLL5
*
long exposure
130-
97-
* Loading control
short exposure

Fig. 3

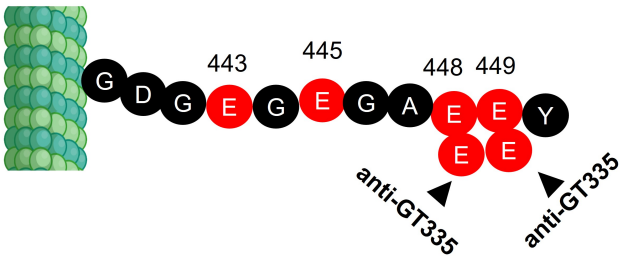

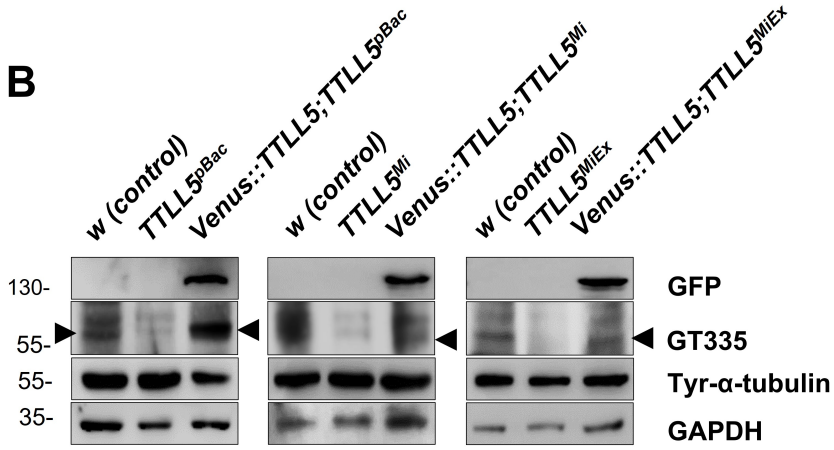

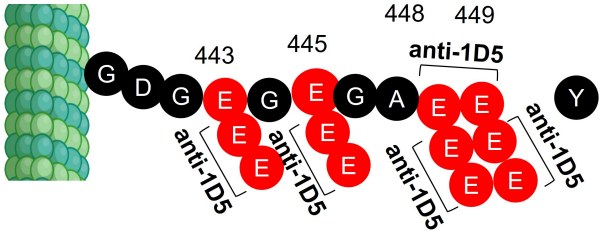

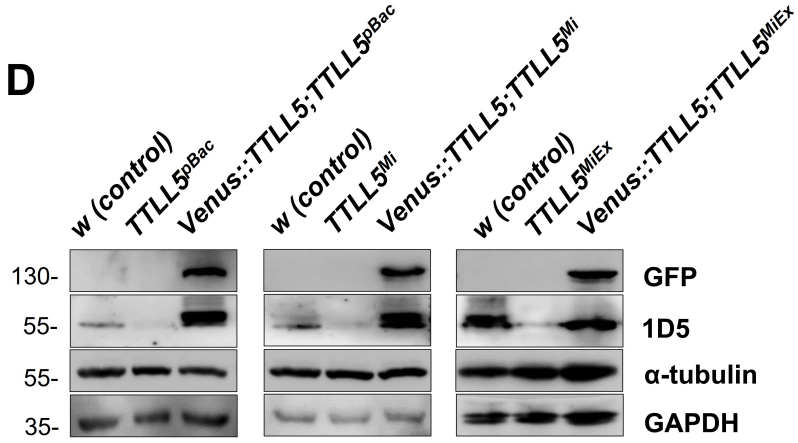

E

Residues of *Drosophila TTLL5*	Function	Corresponding residues in mammalian TTLL5 or TTL	Mutations
E517	ATP/ADP binding	E336 of MmTTLL5 E331 of HsTTL	*WLLE517>S* *E517A*
K282	ATP/ADP binding	K131 of MmTTLL5	*K282 stop codon* *TRK282D>N* *TRK282>KGK*
R339	(In β6-7 loop) stabilizes tubulin to the active site of TTLL5	R188 of MmTTLL5	*R339A*
P522	(Conserved residue of human TTL) anchors TTL to α-tubulin	P336 of HsTTL	*P522A*

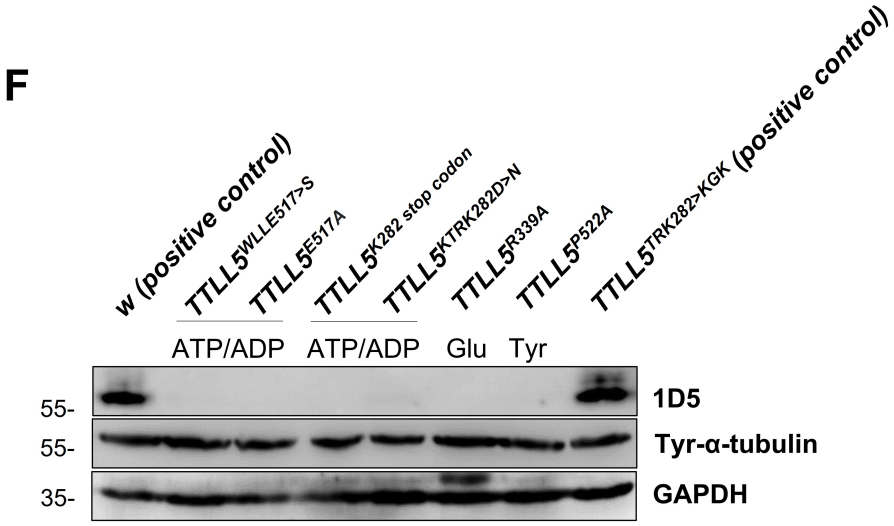

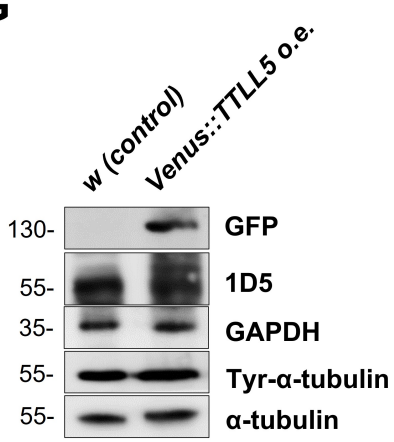

Fig. 4

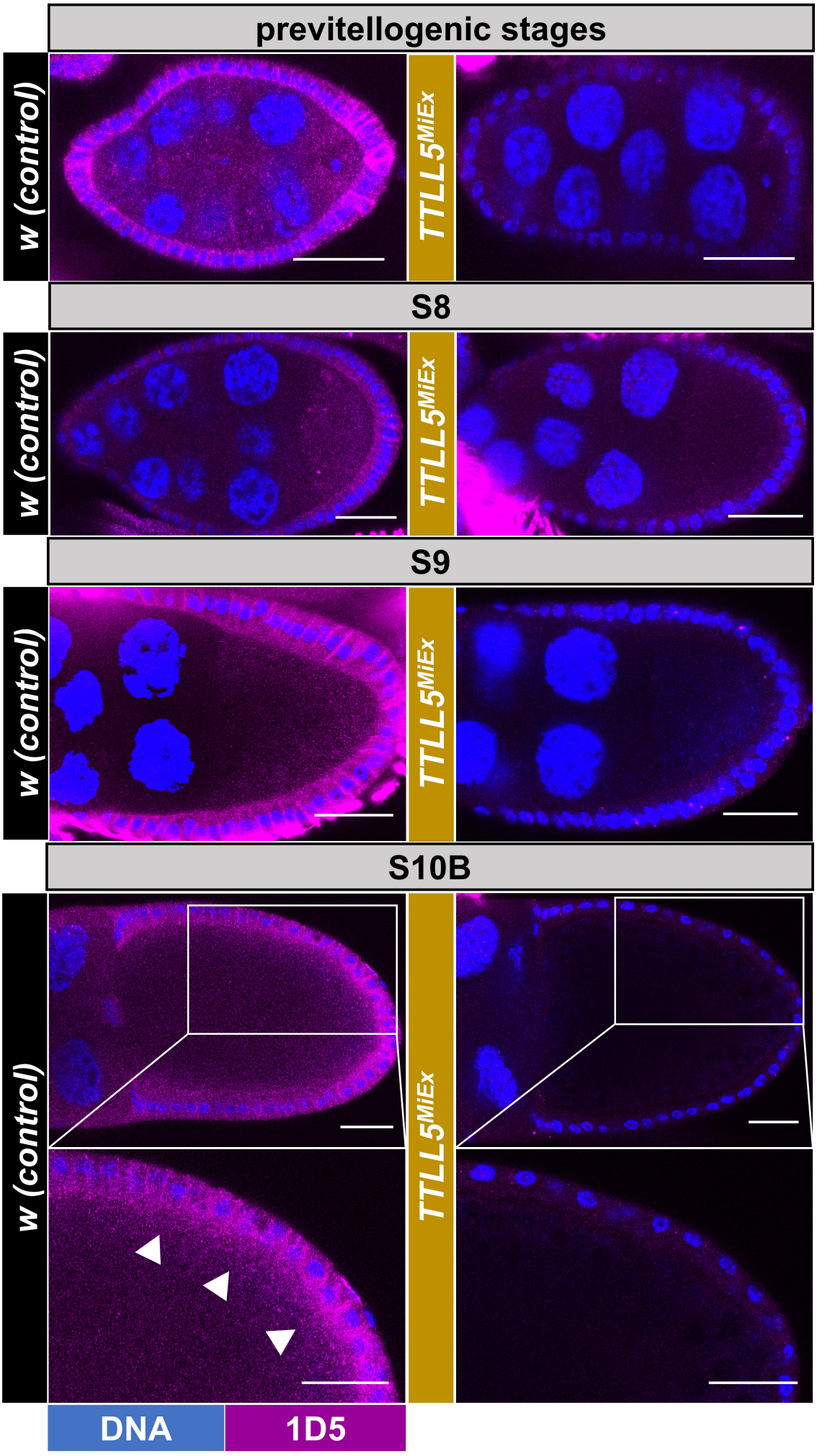
previtellogenic stages
S8
S9
S10B
w (control)
TTLL5MiEx
DNA
1D5

Fig. 5

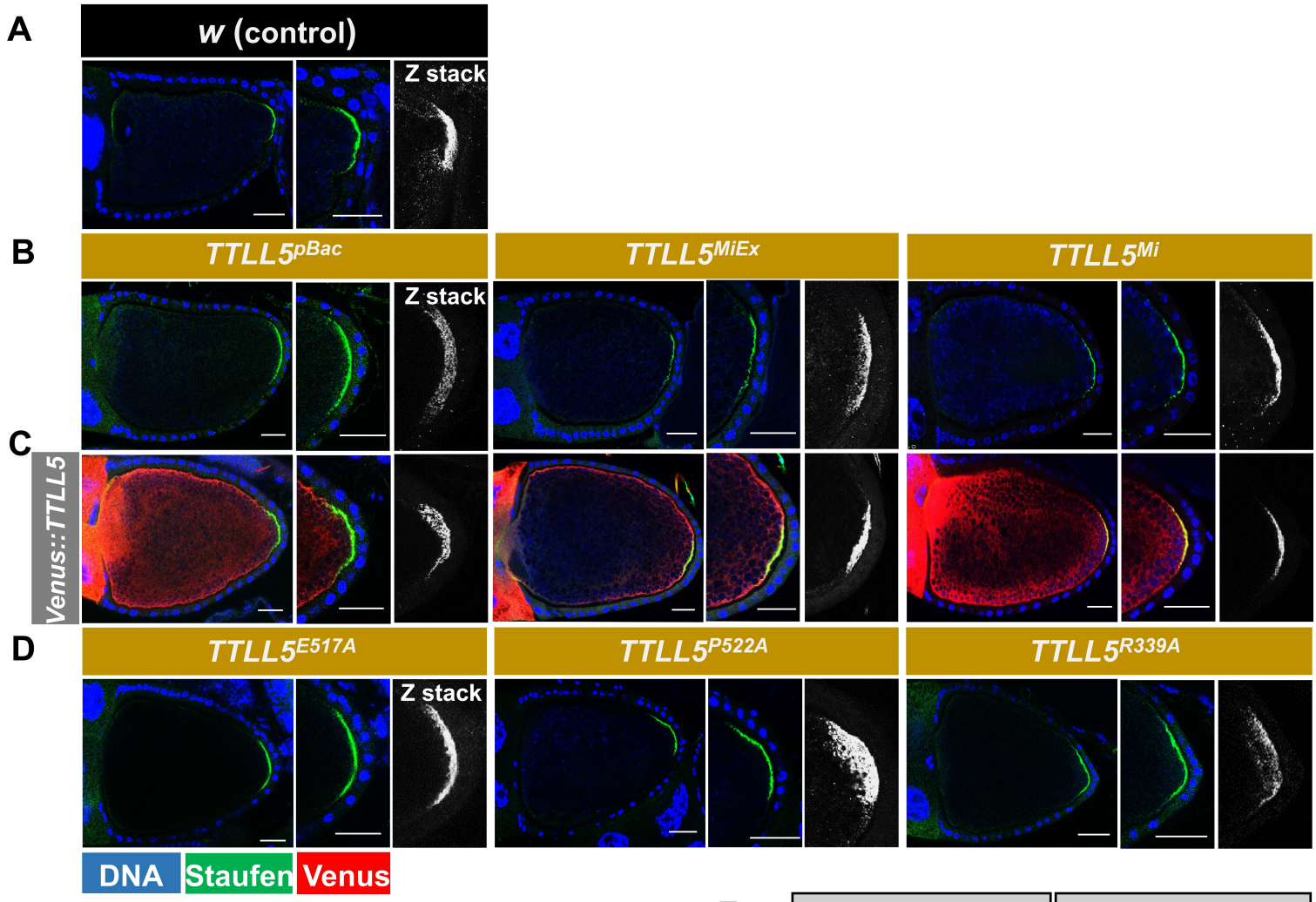
A
w (control)
Z stack
B
TTLL5pBac
TTLL5MiEx
TTLL5Mi
Z stack
C
Venus::TTLL5
D
TTLL5E517A
TTLL5P522A
TTLL5R339A
Z stack
DNA
Staufen
Venus

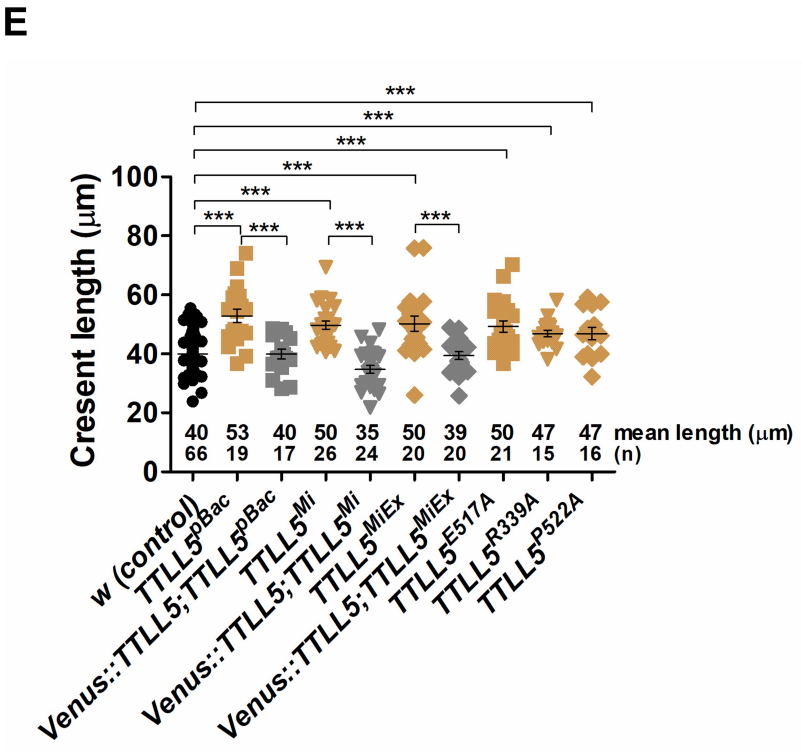
E
Cresent length (μm)
100
80
60
40
20
0
***
40 53 40 50 35 50 39 50 47 47 mean length (μm)
66 19 17 26 24 20 20 21 15 16 (n)
w (control)
TTLL5pBac
Venus::TTLL5;TTLL5pBac
TTLL5Mi
Venus::TTLL5;TTLL5Mi
TTLL5MiEx
Venus::TTLL5;TTLL5MiEx
TTLL5E517A
TTLL5R339A
TTLL5P522A

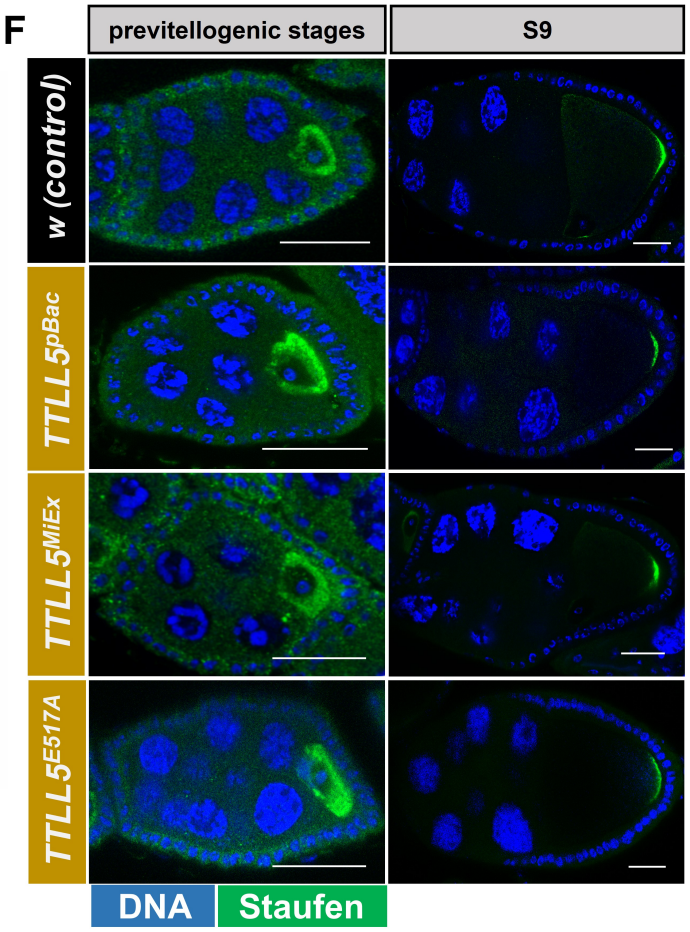
F
previtellogenic stages
S9
w (control)
TTLL5pBac
TTLL5MiEx
TTLL5E517A
DNA
Staufen

Fig. 6

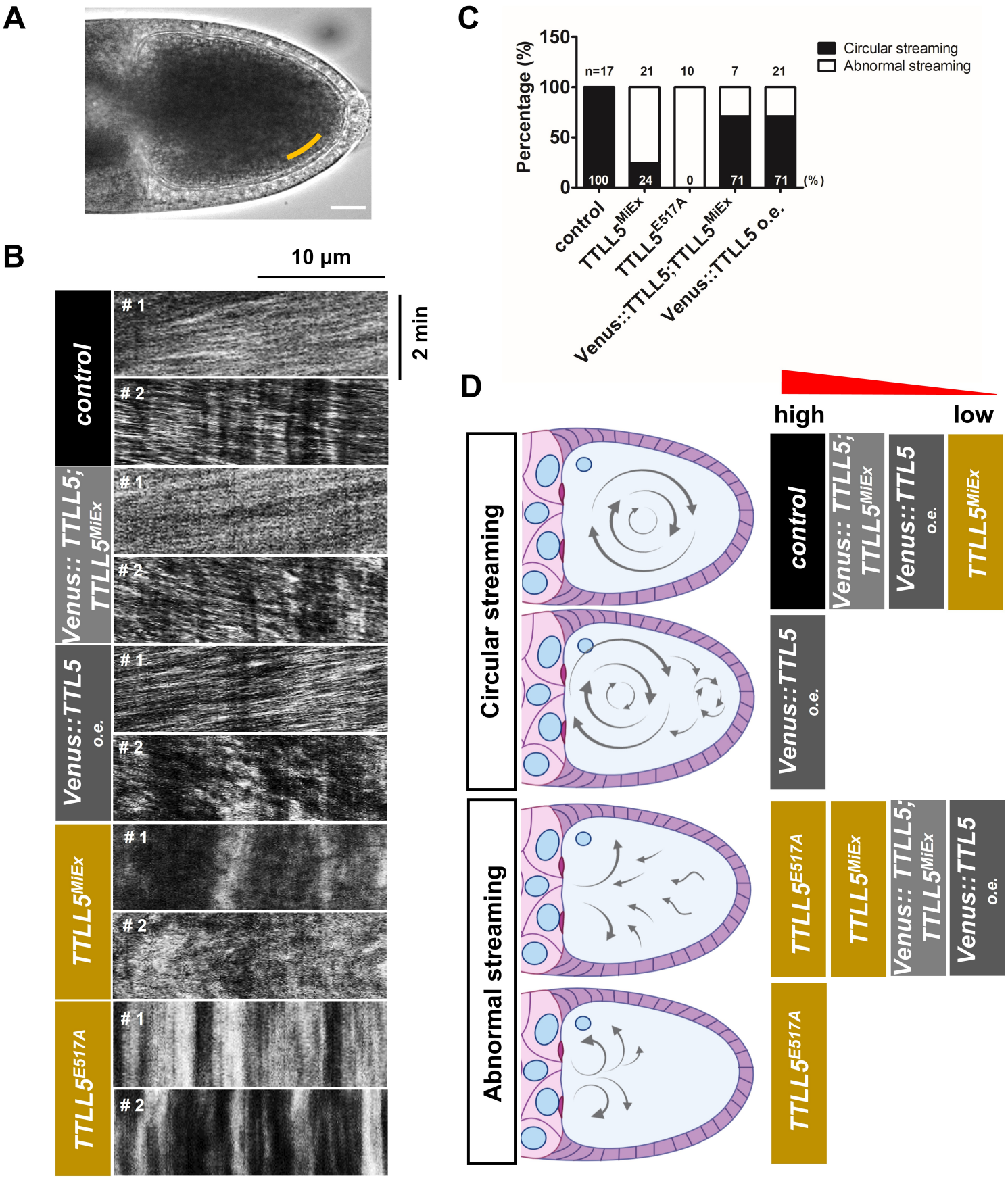
A
B
10 µm
2 min
control
Venus:: TTLL5; TTLL5MiEx
Venus::TTL5 o.e.
TTLL5MiEx
TTLL5E517A
1
2
C
Percentage (%)
150
100
50
0
n=17
21
10
7
21
100
24
0
71
71
(%)
Circular streaming
Abnormal streaming
control
TTLL5MiEx
TTLL5E517A
Venus::TTLL5;TTLL5MiEx
Venus::TTLL5 o.e.
D
Circular streaming
Abnormal streaming
high
low
control
Venus:: TTLL5; TTLL5MiEx
Venus::TTL5 o.e.
TTLL5MiEx
Venus::TTL5 o.e.
TTLL5E517A
TTLL5MiEx
Venus:: TTLL5; TTLL5MiEx
Venus::TTL5 o.e.
TTLL5E517A

Fig. 7

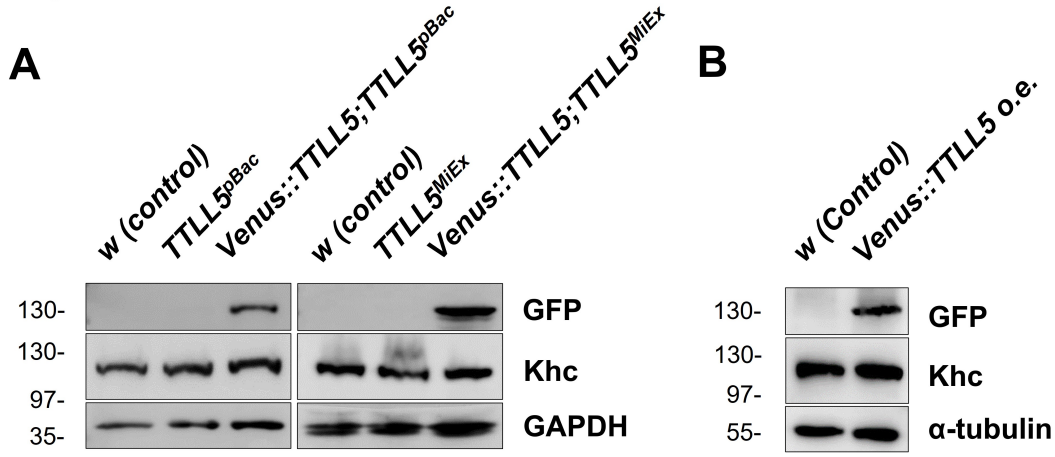
A
w (control)
TTLL5pBac
Venus::TTLL5;TTLL5pBac
w (control)
TTLL5MiEx
Venus::TTLL5;TTLL5MiEx
130-
130-
97-
35-
GFP
Khc
GAPDH
B
w (Control)
Venus::TTLL5 o.e.
130-
130-
97-
55-
GFP
Khc
α-tubulin

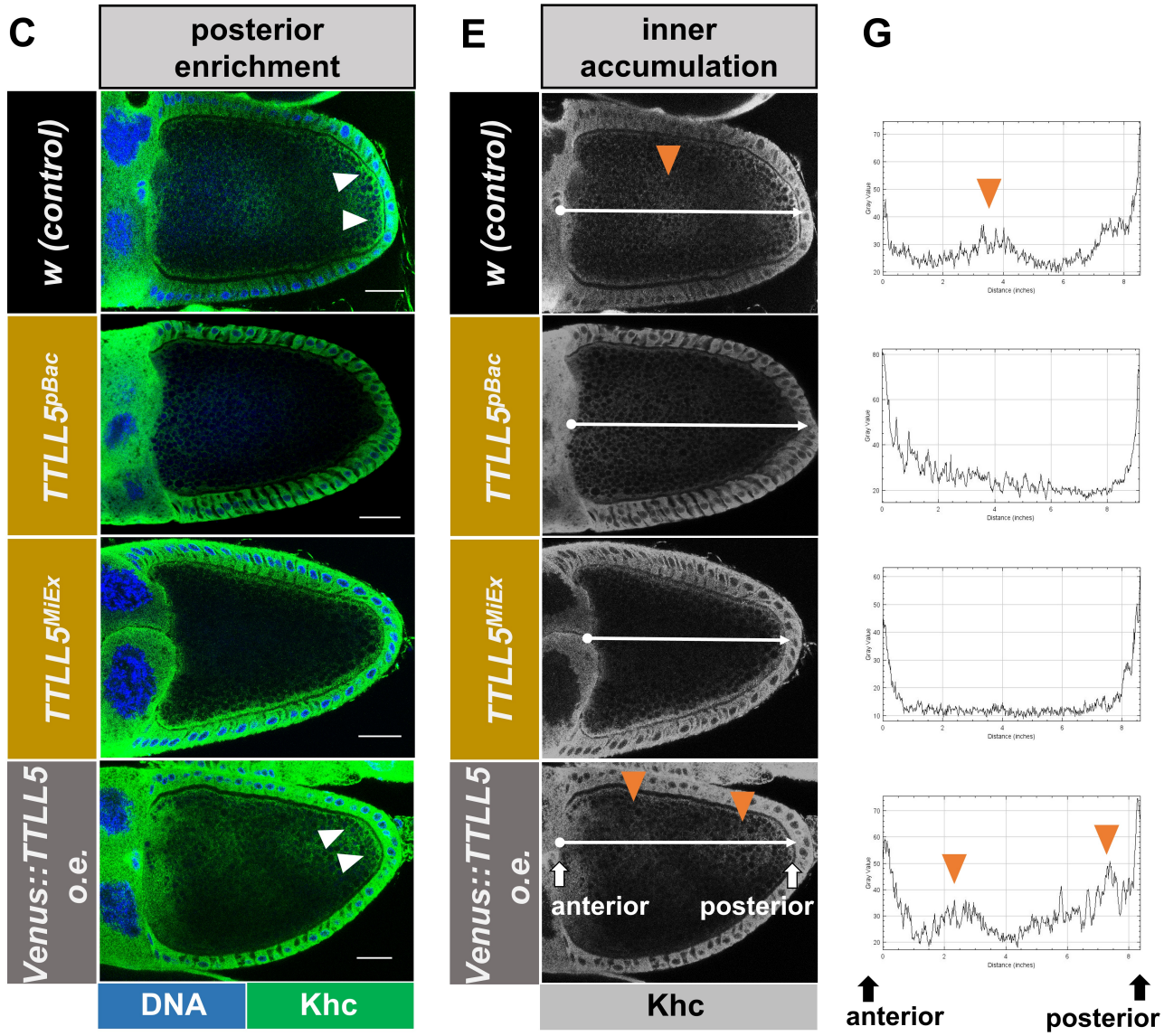
C
posterior enrichment
w (control)
TTLL5pBac
TTLL5MiEx
Venus::TTLL5 o.e.
DNA
Khc
E
inner accumulation
w (control)
TTLL5pBac
TTLL5MiEx
Venus::TTLL5 o.e.
anterior
posterior
Khc
G
anterior
posterior

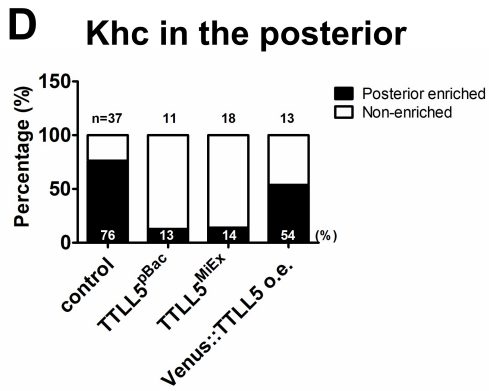
D
Khc in the posterior
Percentage (%)
150
100
50
0
n=37
11
18
13
76
13
14
54
(%)
Posterior enriched
Non-enriched
control
TTLL5pBac
TTLL5MiEx
Venus::TTLL5 o.e.

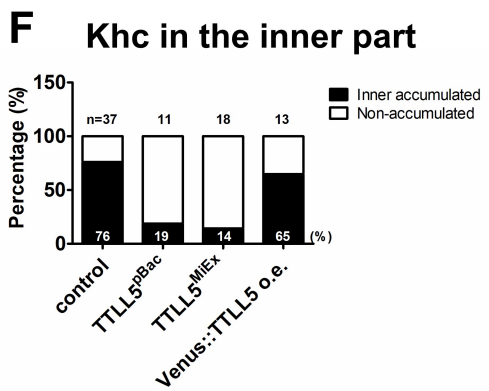
F
Khc in the inner part
Percentage (%)
150
100
50
0
n=37
11
18
13
76
19
14
65
(%)
Inner accumulated
Non-accumulated
control
TTLL5pBac
TTLL5MiEx
Venus::TTLL5 o.e.

Fig. 8

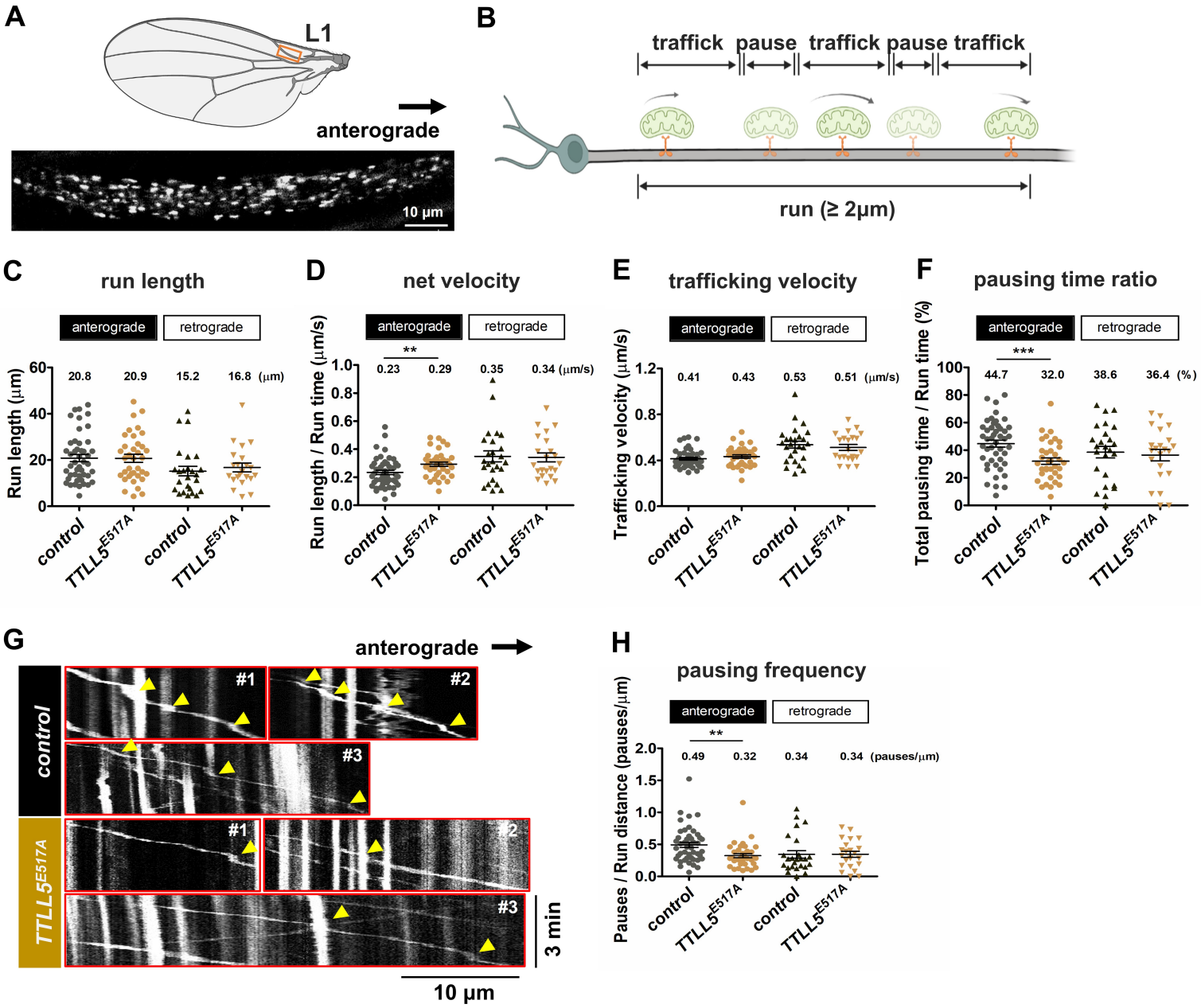
A
L1
anterograde
10 µm
B
traffick pause traffick pause traffick
run (≥ 2µm)
C
run length
anterograde
retrograde
Run length (µm)
20.8 20.9 15.2 16.8 (µm)
control
TTLL5E517A
D
net velocity
Run length / Run time (µm/s)
**
0.23 0.29 0.35 0.34 (µm/s)
E
trafficking velocity
Trafficking velocity (µm/s)
0.41 0.43 0.53 0.51 (µm/s)
F
pausing time ratio
Total pausing time / Run time (%)
***
44.7 32.0 38.6 36.4 (%)
G
anterograde
control
TTLL5E517A
#1
#2
#3
3 min
10 µm
H
pausing frequency
Pauses / Run distance (pauses/µm)
**
0.49 0.32 0.34 0.34 (pauses/µm)

Fig. S1

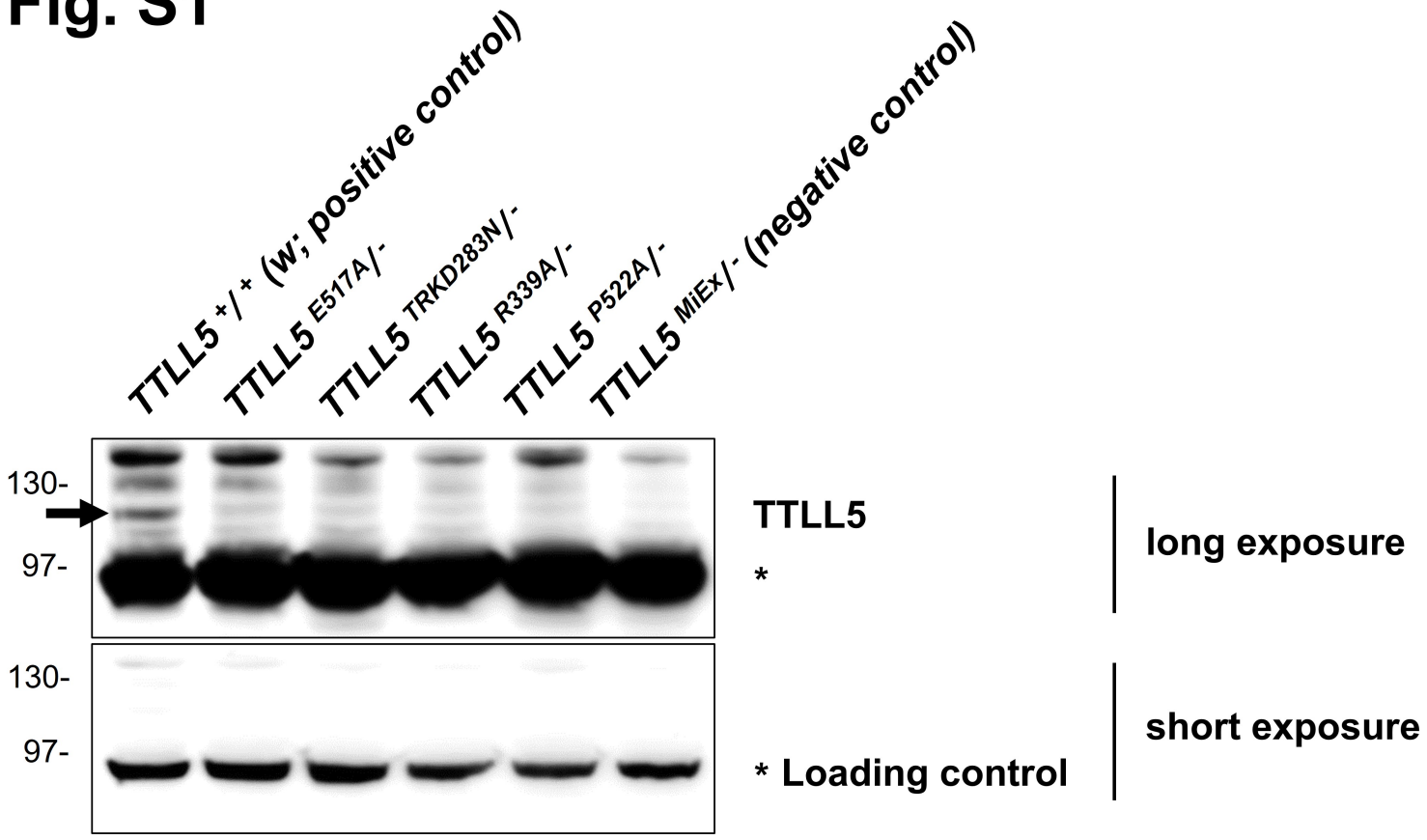
TTLL5 +/+ (w; positive control)
TTLL5 E517A/-
TTLL5 TRKD283N/-
TTLL5 R339A/-
TTLL5 P522A/-
TTLL5 MiEx/- (negative control)
130-
97-
TTLL5
*
long exposure
130-
97-
* Loading control
short exposure

Fig. S2

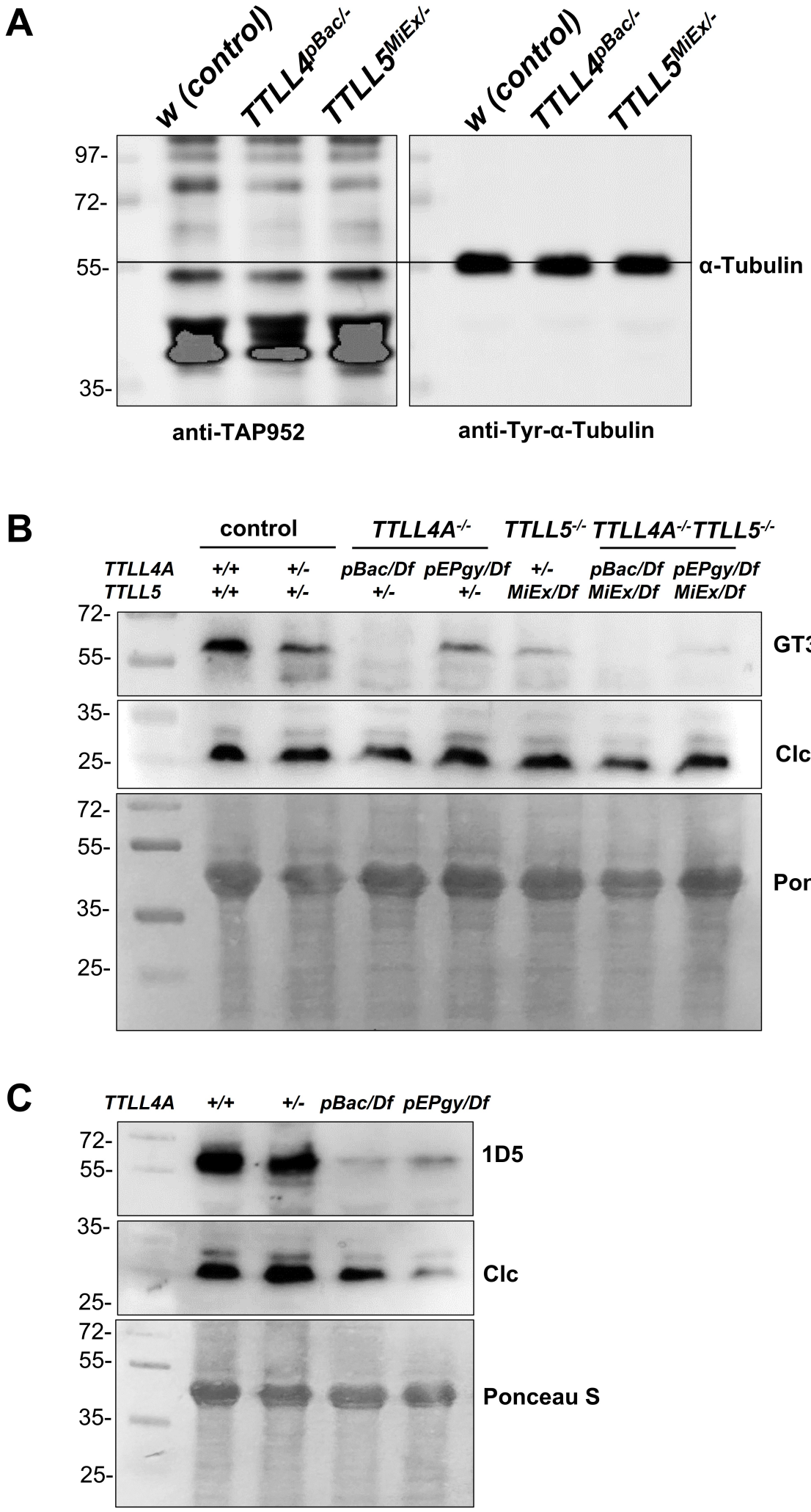
A
w (control)
TTLL4pBac/-
TTLL5MiEx/-
w (control)
TTLL4pBac/-
TTLL5MiEx/-
97-
72-
55-
35-
α-Tubulin
anti-TAP952
anti-Tyr-α-Tubulin
B
control
TTLL4A-/-
TTLL5-/-
TTLL4A-/-TTLL5-/-
TTLL4A +/+ +/- pBac/Df pEPgy/Df +/- pBac/Df pEPgy/Df
TTLL5 +/+ +/- +/- +/- MiEx/Df MiEx/Df MiEx/Df
72-
55-
35-
25-
GT335
Clc
Ponceau S
C
TTLL4A +/+ +/- pBac/Df pEPgy/Df
72-
55-
35-
25-
1D5
Clc
Ponceau S

Fig. S3

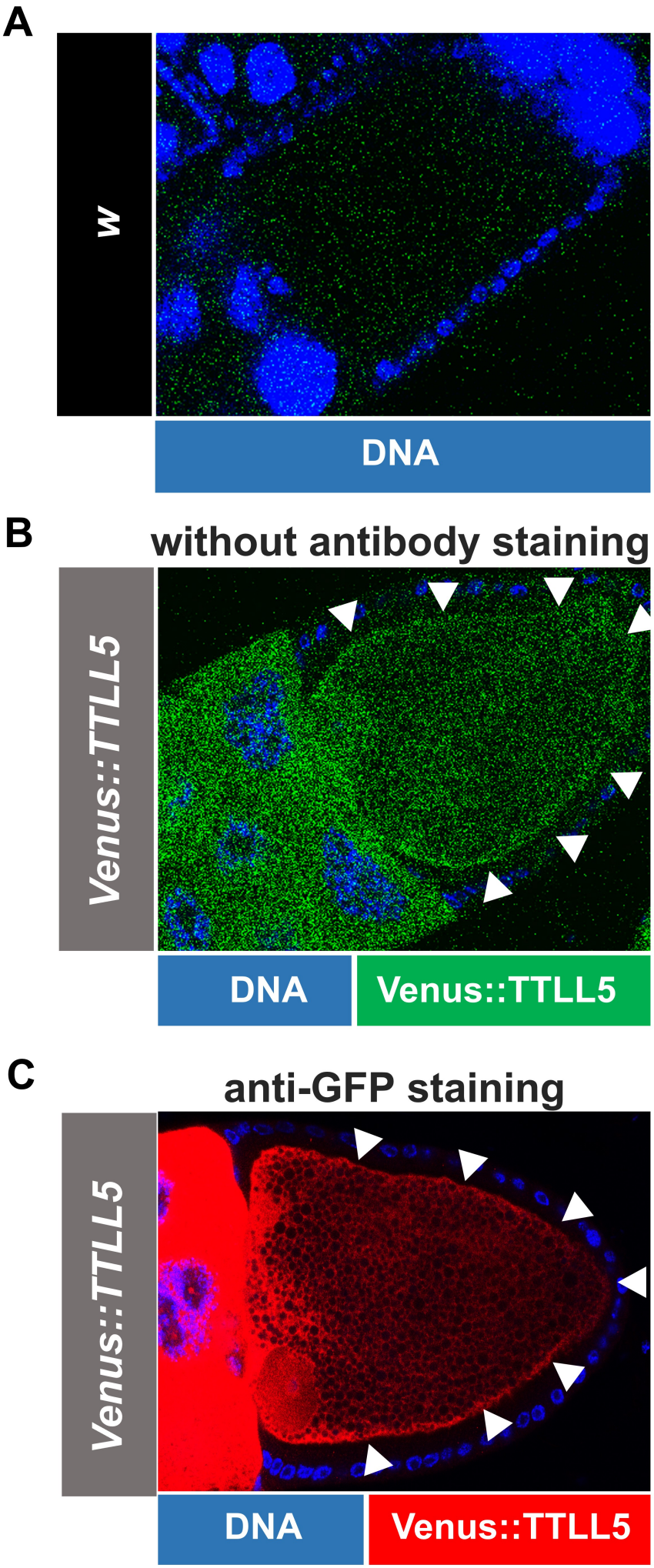
A
w
DNA
B
without antibody staining
Venus::TTLL5
DNA
Venus::TTLL5
C
anti-GFP staining
Venus::TTLL5
DNA
Venus::TTLL5

Fig. S4

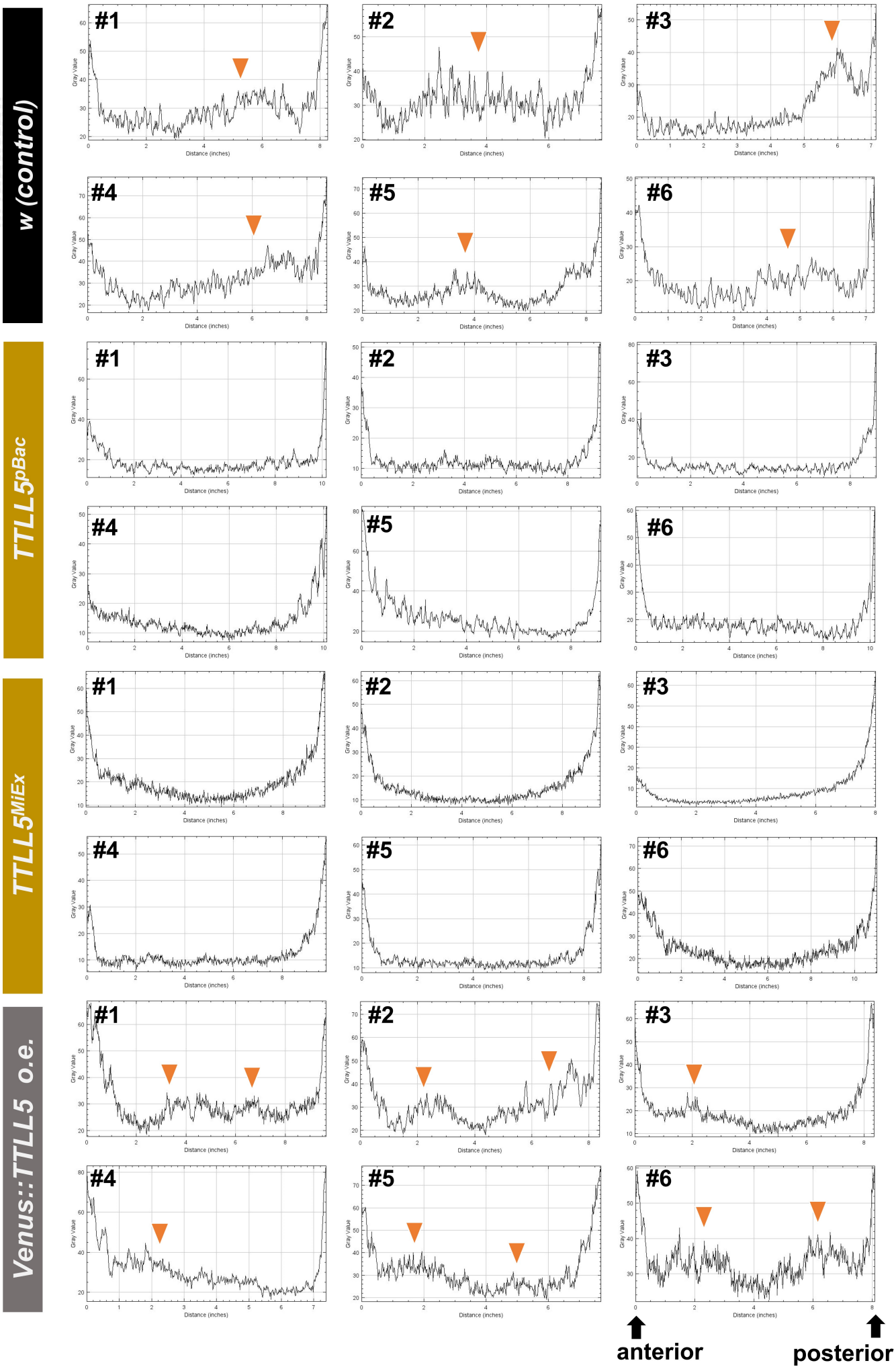
w (control)
TTLL5pBac
TTLL5MiEx
Venus::TTLL5 o.e.
#1
#2
#3
#4
#5
#6
Gray Value
Distance (inches)
anterior
posterior

Fig. S5

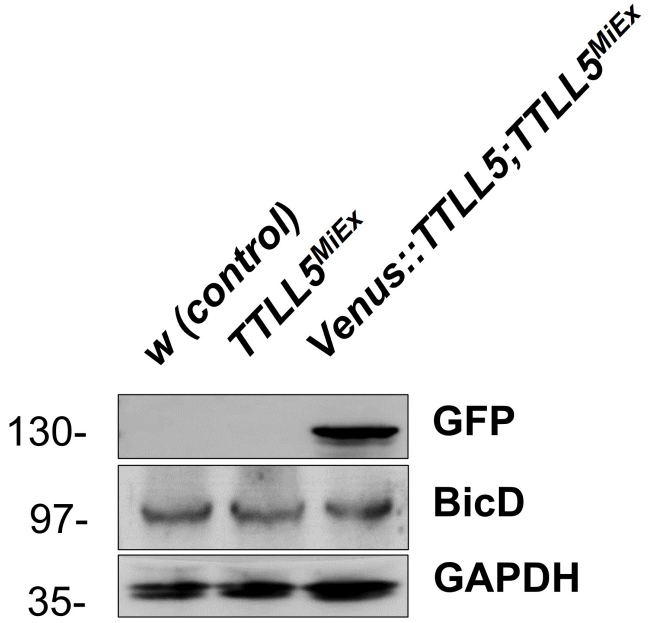
A
w (control)
TTLL5MiEx
Venus::TTLL5;TTLL5MiEx
130-
97-
35-
GFP
BicD
GAPDH

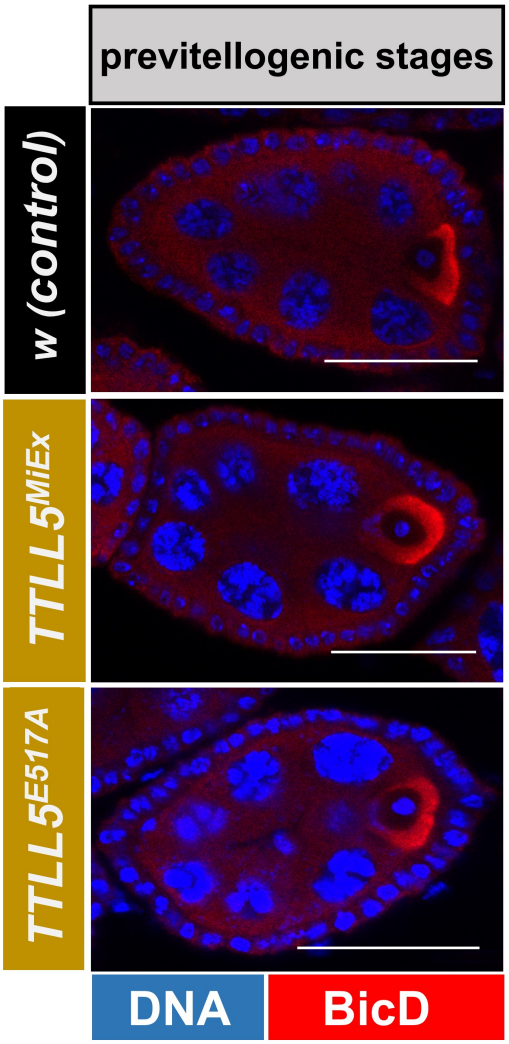
B
previtellogenic stages
w (control)
TTLL5MiEx
TTLL5E517A
DNA
BicD

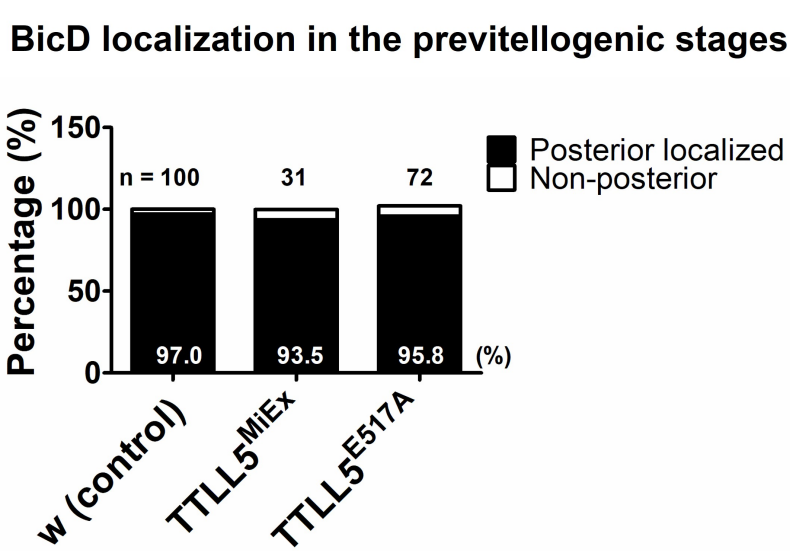
C
BicD localization in the previtellogenic stages
Percentage (%)
150
100
50
0
n = 100
31
72
97.0
93.5
95.8
(%)
Posterior localized
Non-posterior
w (control)
TTLL5MiEx
TTLL5E517A

Fig. S6

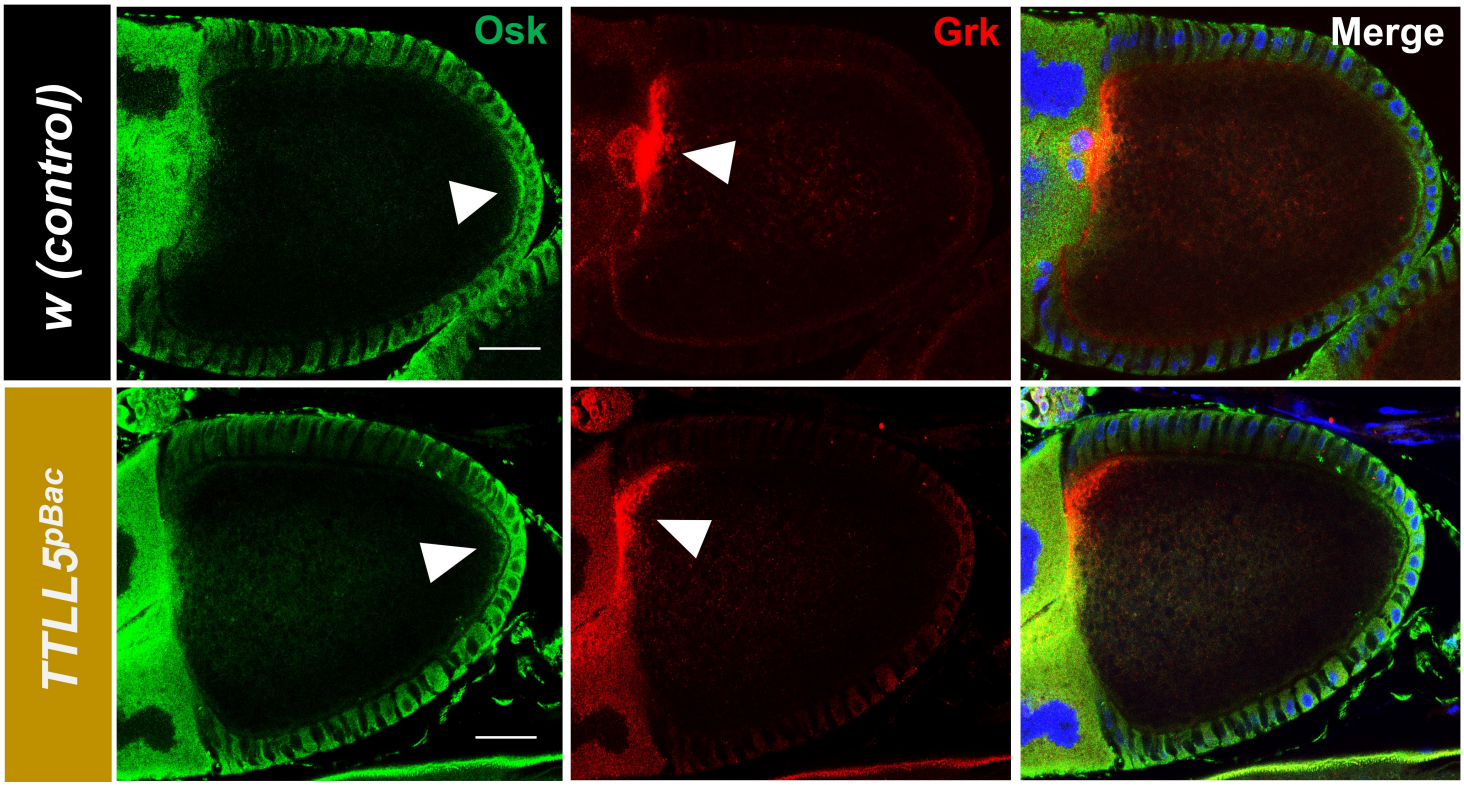

Table S1: Tissue specific expression of the 11 *Drosophila TTLL* genes

Expression levels from high (left column) to low (right column)

TTLL1A	testis	imaginal disc			
TTLL1B	testis	imaginal disc			
TTLL3A					
TTLL3B	testis	imaginal disc	accessory gland	central nervous system	
TTLL4A	testis	imaginal disc	**ovary**	central nervous system	
TTLL4B	testis	imaginal disc	accessory gland	fat body	
TTLL5	**ovary**	imaginal disc	testis	accessory gland	central nervous system
TTLL6A	testis	imaginal disc	accessory gland		
TTLL6B	testis	imaginal disc	accessory gland	fat body	
TTLL12	central nervous system	carcass	**ovary**/head/ imaginal disc	fat body	
TTLL15					

data from FlyBase (https://flybase.org)

Table S2 Number of peptides of αTub84B, αTub84D, and αTub67C found by MS

Isoform	*w*	*TTLL5*^{pBac}	*TTLL5*^{MiEX}
		(PSM value[1)])	
αTub84B/D	56	29	7
αTub67C	12	12	4

[1)] The total peptide numbers were revealed by the values of total PSM (peptide spectrum match) of peptides containing the full primary C-terminal sequence.

Table S3A: primers for cloning the sequences encoding the sgRNAs into the *Drosophila* transformation vector pCFD5

for guide 2	TTLL5 R339 top	5' TGC AGC GGC ATC CAG TCG AGG AAG
	TTLL5 R339 rev	5' AAA CCT TCC TCG ACT GGA TGC CGC
for guide 3	TTLL5 K282 top	5' TGC ATC CTA CGA AAT GAC ACG AA
	TTLL5 K282 rev	5' AAA CTT CGT GTC ATT TCG TAG GA
for guide 4	TTLL5 E517 top	5' TGC AAG ATT GAT TTC CAG TAG CCA
	TTLL5 E517 rev	5' AAA CTG GCT ACT GGA AAT CAA TCT
for guide 5	TTLL5 R376 top	5' TGC ATG GTC ACA AAT GTG ATT TGA
	TTLL5 R376 rev	5' AAA CTC AAA TCA CAT TTG TGA CCA

Table S3B: templates to introduce point mutations

TTLL5^{R339A}
= Arg (AGG) -> Ala (**GCT**) on the reverse strand; introducing an AluI site (AGCT) at the same time; PAM (underlined) on the other strand (5'TGG) 5'GAATTATAGCAAGTTGTTGGTTTAGTTACCGAATTAACAATAAATATTCC**AGC**T'CCTCGACTGGATGCCGCTGGCTTAACTATCCATGGTCCGCGATGCTTGTT
TTLL5^{E517A}
= Glu (GAA) -> Ala (**GCC**) on the reverse strand; introducing a HaeIII site (GGCC) at the same time; PAM (underlined) on this strand (5'TGG) 5'ACCTTAGTGTCCAAAGGACTATCCACACCCATTGACGGCGATAGATTGAT**GGC**CAGTAG'CCATGGCTTAAGTGCGTTGTCTATTAATATATCGAATCCATACAGCTCAA
TTLL5^{P522A}
= Pro (CCG) -> Ala (GCG) on the reverse strand; introducing a BsaHI site (GRCGYC) at the same time; PAM (underlined) on this strand (5'TGG); grey nucleotide changes that are silent mutations to prevent multiple recognition after DNA was cut 5'GTCTGCCATCAGACATGACTTAACCTTAGTGTCCAAAGGACTATCCACACCCATTGA**CGC**CGATAGATTGATTTC**G**AG**A**AG'CCATGGCTTAAGTGCGTTGTCTATTAATATATCGAATCCATACAGCTCAA

Fig. S1: TTLL5 was stably expressed in all Crispr/Cas9 generated *TTLL5* mutants. All Crispr/Cas9 generated *TTLL5* mutations were analyzed hemizygously over *Df(3R)BSC679.* TR**K**D283N refers to a more complex mutation in which the 4 codons TR**K**D283 were replaced by a single N. We expect extracts from these animals to contain at most half the normal amount of TTLL5. *w* ($TTLL5^{+}/TTLL5^{+}$) was the positive control and the null mutation $TTLL5^{MiEx}/Df(3R)BSC679$ was the negative control. The signal of an unspecific band (labeled with *) under short exposure was treated as a loading control. *w,* which contains 2 copies of the $TTLL5^{+}$ allele expressed the highest levels of TTLL5. Crispr/Cas9 generated *TTLL5* mutants with a single allele of *TTLL5** expressed less TTLL5 compared to *w,* but more compared to the null mutant $TTLL5^{MiEx}/Df(3R)BSC679$. The TTLL5 levels of the hemizygous point mutants were similar to the ones of the hemizygous $TTLL5^{+}$ (see **Fig. 2B**). The faint band seen in $TTLL5^{MiEx}/Df(3R)BSC679$ is probably a background band.

Fig. S2: Preliminary studies on the role of *TTLL4* in α-tubulin modification in the *Drosophila* ovaries. A) The glycylation of α-tubulin was evaluated by Western blotting with the anti-monoglycylated Tubulin antibody TAP952. The anti-Tyr-α-Tubulin was a loading and size control. TAP952 did not detect a clear band in the α-Tubulin region in the wild type, *TTLL4A* or *TTLL5* mutant. B) Preliminary results indicate that *TTLL4A* is required for monoglutamylation and polyglutamylation of α-tubulin in ovaries. The monoglutamylation was evaluated by Western blotting with GT335 antibodies. The relative signal of GT335 is strongly reduced in $TTLL4A^{pBac}$, $TTLL5^{MiEx}$, $TTLL4A^{pBac};TTLL5^{MiEx}$, $TTLL4A^{pEPgy};TTLL5^{MiEx}$ mutants compared to controls. GT335 signal is slightly reduced in $TTLL4A^{pEPgy}$ mutant. $TTLL4A^{pEPgy}$ is an insertion into the promoter region and appears to be a hypomorphic mutation while the $TTLL4A^{pBac}$ allele is an insertion into the leader and appears to be the stronger loss-of-function allele. Note that the lack of a GT335 signal in the $TTLL4A^{-/-}$; $TTLL5^{+/-}$ is inconsistent with other results showing the role of *TTLL5* in monoglutamylation. Additional work is needed to find out what the reason for this is. C) The relative polyglutamylation signal visualized by the 1D5 antibodies is strongly reduced in the $TTLL4A^{pBac}$ mutant and also reduced in $TTLL4A^{EPgy}$. Ponceau S and Clc were treated as loading controls. The *TTLL5* allele was analyzed in hemizygous animals over *Df(3R)BSC679*. All *TTLL4A* alleles were hemizygous over *Df(2L)BSC145.* The genotype for controls were *w* (+/+), and *+/Df(2L)BSC145 or* $TTLL4A^{pBac}$*;+/ Df(3R)BSC679 or* $TTLL5^{MiEx}$.

Fig. S3: *Venus::TTLL5* expression in S10 oocytes. Confocal micrographs showing the S10 oocyte with or without anti-GFP staining. A) *w* oocyte shows the autofluorescence background of the oocyte under the microscope. B) The oocyte overexpressing

Venus:TTLL5 shows the live fluorescence of Venus (green). C) The oocyte overexpressing *Venus:TTLL5* shows the Venus::TTLL5 protein after staining with an anti-GFP antibody (red). Hochest was in blue. The cortical signal of Venus::TTLL5 in the oocytes is pointed out with white arrowheads. The genotype for *Venus:TTLL5* overexpression was *MattubGal4/UAS-Venus::TTLL5.*

Fig. S4: Khc distribution in S10B oocytes. Intensity charts from 6 samples of each genotype were plotted based on the line drawn along the AP axis of S10B oocytes (see Fig. 7E). The orange triangles in the control and *o.e. Venus::TTLL5* point out the inner regions accumulating higher levels of Khc. The control was *w* or *+/Df(3R)BSC679.* Genotypes for *TTLL5* mutants: *MattubGal4/+;TTLL5^{pBac}/Df(3R)BSC679* and *TTLL5^{MiEx}/Df(3R)BSC679*, respectively. Genotype for *TTLL5* overexpression: *MattubGal4/UAS-Venus::TTLL5.*

Fig. S5: *TTLL5* has little or no effects on BicD expression and distribution in ovaries. A) BicD levels remained unchanged between the *w* control, a *TTLL5* deficiency mutant and the *TTLL5* rescue strain. GAPDH served as the loading control. B) Confocal micrographs show BicD localizing preferentially at the posterior of the previtellogenic oocytes of *w* controls and *TTLL5* mutants. Scale Bar: 25µm. BicD protein in red, and Hoechst in blue. C) 97%, 93.5% and 95.8% of the oocytes showed posteriorly localized BicD in the *w* control, *TTLL5^{MiEx}* and *TTLL5^{E517A}* mutants, respectively. The total numbers of early oocytes are indicated as n= in the chart. Genotype for control: *w* or *+/Df(3R)BSC679.* Genotypes for *TTLL5* mutants: *TTLL5^{MiEx}/Df(3R)BSC679* and *TTLL5^{E517A}/Df(3R)BSC679*, respectively.

Fig. S6: The polarity of S10B oocytes is normal in *TTLL5* mutant. In *TTLL5^{pBac}* oocytes, Gurken (red) localizes properly to the dorsoanterior part of the oocyte cortex and Oskar (green) to the posterior cortex of 10B stage oocytes, indicating the polarity of MTs at this stage was normal. Blue channel: DNA. Genotypes for *TTLL5^{pBac}*: *TTLL5^{pBac} /Df(3R)BSC679.*

Mov. S1: Ooplasmic streaming in *w* (control; 2 oocytes)
Mov. S2: Ooplasmic streaming in *TTLL5^{MiEx}* (2 oocytes)
Mov. S3: Ooplasmic streaming in *TTLL5^{E517A}* (2 oocytes)
Mov. S4: Ooplasmic streaming in *Venus::TTLL5; TTLL5^{MiEx}* (2 oocytes)
Mov. S5: Ooplasmic streaming in *Venus::TTLL5* (2 oocytes)
Mov. S6: Appl-Gal4>Mito::GFP trafficking in the L1 vein. Top movie: control; bottom movie: *TTLL5^{E517A}*.